Polynomial chaos kriging-assisted reliability-based design optimization for a deep mixing wall

Tingting Zhang, Adel Abdallah, Olivier Cuisinier, Farimah Masrouri

Polynomial Chaos Kriging-assisted reliability-based design optimization for a Deep Mixing Wall

Tingting Zhang [a]*, Adel Abdallah [a], Olivier Cuisinier [a], Farimah Masrouri [a]

[a] Université de Lorraine, LEMTA (UMR 7563) CNRS, 2 Av. de la Forêt de Haye, 54500 Vandœuvre-lès-Nancy, France
*Corresponding author at: Laboratory LEMTA (UMR 7563) CNRS, Université de Lorraine. Address: 2 Av. de la Forêt de Haye, 54500 Vandœuvre-lès-Nancy, France. Email: tingting.zhang@univ-lorraine.fr

Abstract

This paper presents a Reliability-Based Design Optimization (RBDO) for Deep Mixing Walls (DMW), taking into account parameter uncertainties, required safety levels and construction costs. A procedure that integrates Polynomial Chaos Kriging (PCK) and constrained (1+1) Covariance Matrix Adaptation Evolution Strategy (constrained (1+1)-CMA-ES) is proposed, referred to as PCK-RBDO-ES, for the optimization of DMW design. Specifically, PCK is employed to reduce required numerical simulations and improve efficiency of reliability assessments, while the constrained (1+1)-CMA-ES method is used for global optimization of design parameters. Unconfined Compressive Strength (UCS) is considered as the design variable to be optimized in this study and an existing DMW was selected as a reference case. The PCK-RBDO-ES results are first presented and compared to validate the effectiveness and efficiency. Then, the influence of the DMW uncertainties and adjacent soil uncertainties on the UCS evaluations is discussed, and the effect of the target reliability requirement is further investigated. The results indicate that the proposed PCK-RBDO-ES procedure is effective and provides useful insights for DMW design and construction. Uncertainties on UCS and stiffness of DMW, as well as on the friction angle of soft to medium clay layer, are shown to have significant impacts on the design optimization. This study can help designers to manage project risks, and facilitate risk-aware and cost-effective decision-making.

Keywords

Deep Mixing Wall; Reliability-Based Design Optimization; Polynomial Chaos Kriging; Constrained (1+1)-CMA-ES; Unconfined Compressive Strength.

Nomenclature

Abbreviations presented in this paper:

CDF	Cumulative Distribution Function
CMA-ES	Covariance Matrix Adaptation-Evolution Strategy
Constrained (1+1)-CMA-ES	Constrained (1+1) Covariance Matrix Adaptation-Evolution Strategy
COV	Coefficient Of Variation
DBDO	Deterministic-Based Design Optimization
DMW	Deep Mixing Wall
ED	Experimental Design
FC	Fill Crust
FEM	Finite Element Method
HSS	Hardening Soil Model with Small Strain Stiffness
LHS	Latin Hypercube Sampling
LOO	Leave-One-Out Error
MCS	Monte Carlo Simulation
OCR	Over Consolidation Ratio
PCE	Polynomial Chaos Expansion
PCK	Polynomial Chaos Kriging
PDF	Probability Density Function
PMA	Performance Measure Approach
RBDO	Reliability-Based Design Optimization
RIA	Reliability Index Approach
SC	Stiff Clay
SLS	Serviceability Limit State
SMC	Soft to Medium Clay
UCS	Unconfined Compressive Strength
ULS	Ultimate Limit State
VSC	Very Stiff Clay

1. Introduction

Utilizing underground space is increasingly popular as an eco-friendly solution to alleviate land scarcity in urban areas, with excavation construction being an important component of underground

infrastructure development. Excavation design and construction face challenges due to growing urban demands, stricter displacement limits, and stringent regulations on noise and pollution, especially in densely populated areas. Deep Mixing Wall (DMW), created by mechanically blending cement with in-situ soil to form a reliable barrier against groundwater infiltration and provide structural support for underground excavations, is an attractive option for urban excavation projects (Waichita et al., 2019; Wang et al., 2010). They are favored for their environmental friendliness, cost-effectiveness, quick construction time, minimal disruption to the surrounding area, low maintenance requirements and versatility. DMWs have been successfully utilized in various countries, such as Belgium (Denies et al., 2012), France (Peixoto et al., 2012), China (Wang et al., 2010) and Thailand (Jamsawang et al., 2019; Waichita et al., 2020, 2019), demonstrating their effectiveness and applicability across different regions. Several relevant studies have been conducted to analyze the DMW stability and discuss the effects of the relevant DMW shape, strength and stiffness on DMW stability (Jamsawang et al., 2019, 2017; Shao et al., 2005; Voottipruex et al., 2019; Waichita et al., 2021, 2020, 2019; Yamashita et al., 2011).

The above-mentioned DMW studies provide good insights into the DMW design and construction. However, it is noted that the existing researches are conducted within a deterministic framework, whereas in practice, significant uncertainties and spatial variabilities in the DMW properties (such as strength, stiffness and permeability) can arise due to the complicated construction process (mixing and curing conditions), the natural variability of in-situ soil (complex geological composition), potential measurement errors (limited data availability, equipment constraints, and random testing), construction techniques and workmanships (Filz and Navin, 2010; Phutthananon et al., 2023; Spross et al., 2021). These factors can significantly influence the quality and the mechanical behavior of DMWs and may result in discrepancies between design results and field observations. Therefore, adopting a reliability analysis to account for these uncertainties, is more rational for DMW stability assessment and quality control to avoid and mitigate the risks (Das and Das, 2010; Larsson and Bergman, 2015; Phutthananon et al., 2023). Additionally, economic factors play a crucial role in engineering design and should be explicitly considered to avoid designs that are “overly safe (low risk) but high cost” or “economical but unsafe (high risk)” (Hoy et al., 2023; Zhao,

2022). Consequently, it is essential to ensure that DMWs are designed and constructed to be both economical and safe while considering the uncertainties. However, this aspect is rarely addressed in existing studies to the knowledge of the authors and will be explored in this study.

Reliability-Based Design Optimization (RBDO), which accounts for uncertainty all along the optimization process, is introduced to develop a design that minimizes the DMW construction costs while meeting safety requirements effectively (Huang et al., 2022; Khorramian et al., 2023; Liu et al., 2023; Marelli and Sudret, 2014). Three main methods have been developed to address RBDO problems, including (i) the double-loop approach which consists of two nested loops: an inner loop for the reliability assessment and an outer loop for the design optimization, (ii) the single-loop approach which integrates reliability assessment into the optimization loop, thus eliminating the need for separate reliability assessment loops, and (iii) the decoupled approach which separates the optimization and reliability assessment processes, typically performing optimization first and then conducting reliability analysis on the optimized design (Dubourg et al., 2011; Moustapha and Sudret, 2019). Compared to the double-loop method, the single-loop and decoupled approaches are more efficient. However, they are not always effective and may fail to converge when the starting point of the optimization problem is far from the optimal solution (Moustapha and Sudret, 2019). Conversely, the double-loop method is more commonly used due to its conceptual simplicity, high accuracy and versatility (Okoro et al., 2023). However, it is noted that the double-loop method has its limitations in terms of efficiency as it requires multiple reliability analyses, particularly for complex real-world projects involving time-consuming numerical simulations or complex computations (Lü et al., 2017; Marelli and Sudret, 2014). To tackle this challenge, several methods have been proposed to enhance the efficiency of RBDO analyses, including the Reliability Index Approach (RIA) and the Performance Measure Approach (PMA), which incorporate the approximation reliability methods (such as First Order Reliability Method) into the inner loop to reduce the number of required evaluations in the reliability analysis. However, the approximation reliability methods may lead to biased results when dealing with problems with highly non-linear limit-state surfaces (Dubourg et al., 2011; Lü et al., 2017; Zhao, 2022).

Furthermore, the optimized outcomes derived from the RIA and PMA methodologies are greatly influenced by the initial design configurations, which heavily depend on prior experiences (Lü et al., 2017).

Alternatively, the surrogate model, which is a simplified or approximated model used to represent the behaviour of a more complex system (Zhang, 2023), is widely used in the reliability analysis of geotechnical structures, such as tunnels (Guo et al., 2019; Man et al., 2023), circular shafts (Zhang et al., 2022), slopes (Sun et al., 2023) and dams (Guo and Dias, 2020). This is because once the surrogate model is constructed well with a limited number of samples, there is no need to do more deterministic numerical evaluations for the reliability analysis, thus significantly reducing computational costs. Among the commonly used surrogate models (such as the Polynomial Chaos Expansion: PCE, Kriging, Polynomial Chaos Kriging: PCK, and machine learning models), the PCK shows a great performance in terms of the accuracy and efficiency of the surrogate model construction as it integrates the advantages of the PCE and Kriging, and it is accepted that the PCK permits to build a more efficient and accurate metamodel compared to PCE and Kriging separately (Man et al., 2023; Marelli and Sudret, 2014). Besides, compared to the machine learning model, which requires an extensive dataset preparation beforehand and hyperparameter tuning during the model construction, the PCK approach leverages a local variance estimator for an adaptive learning process (Li et al., 2021; Qu et al., 2023). This allows the sample set used for metamodel construction to be enriched iteratively, ensuring an optimal balance between model accuracy and computational efficiency. As a result, the PCK is integrated into the RBDO analysis in this study to enhance the efficiency of reliability analysis within the inner loop.

In addition, the optimization in the outer-loop, which aims to find the optimal design parameters that minimize the overall cost while satisfying the reliability requirements defined in the inner loop, is the other concern in RBDO analysis. Compared to the local minimization methods (such as sequential quadratic programming), which rely on local information and are likely to converge to a local solution (getting trapped in local optima), the global optimization techniques (such as genetic algorithms, simulated annealing, particle swarm optimization and evolutionary strategies) can explore the entire design domain and are more likely to find the global solutions (Marelli and Sudret, 2014). The constrained (1+1)-Covariance Matrix

Adaptation-Evolution Strategy (constrained (1+1)-CMA-ES), is introduced and carried out for the design parameters optimization due to its adaptability and robustness, and has the ability to handle complex optimization problems, including those with nonlinear, non-convex and high-dimensional objective functions (Arnold and Hansen, 2012). The basic idea of the algorithm is to sample points in the search space and adapt the sampling mechanism so as to iteratively move towards the optimal solution.

In general, a PCK-RBDO-ES procedure is proposed for efficient DMW design and construction, where a surrogate model PCK is constructed to replace the time-consuming deterministic model, and the constrained (1+1)-CMA-ES is implemented to optimize the DMW design. This paper starts with an introduction of the reference case, a DMW in Bangkok, which is previously investigated by Waichita et al. (2019). After constructing and validating the deterministic model, the PCK-based DMW design optimization is explained, followed by an introduction of the PCK-RBDO-ES procedure, along with the related flowchart. The application of PCK-RBDO-ES to the DMW case is then presented and its effectiveness is also investigated. Additionally, some discussions are then conducted benefiting from the efficiency of the PCK-RBDO-ES, which aims to provide more practical insights.

Compared to the existing studies, the advantages and contributions include: (i) the DMW design and construction takes into account the parameter uncertainties, required safety levels and construction costs, which is more rational and cost-effective; (ii) PCK-assisted RBDO enhances computational efficiency and is available for the practical applications; (iii) constrained (1+1)-CMA-ES, known for its adaptability and robustness, is employed to accomplish the global optimization; (iv) several discussions are given in terms of the DMW uncertainties, soil uncertainties and target safety requirements, which provide more insights for practical engineering.

2. Problem statement

It is noted that in addition to laboratory and field experiments (Denies and Huybrechts, 2017; Waichita et al., 2021; Yamashita et al., 2011), numerical simulations are also of interest due to their greater flexibility, effectiveness and versatility, which is employed in this study for the DMW stability analysis (Jamsawang

et al., 2019, 2017; Waichita et al., 2020). This section provides an overview of the studied DMW reference case and the corresponding numerical model construction, which follows by the relevant statistical information of the considered variables. The design optimization of the RBDO is also introduced.

2.1 Finite element modelling

A DMW in Bangkok previously examined by Waichita et al. (2019) is the reference case in this study. The wall consists of three 15 m-deep, 1 m-diameter DCM columns overlapping by 0.1 m to form a 2.8 m-thick wall. The excavation is of 5 m depth and 27 m width, and the groundwater table is 1 m below the ground surface. A plane-strain Finite Element Model (FEM) is constructed by Plaxis 2D (2022) and is presented in Fig. 1. One-half of the cross-section is modeled to benefit from the vertical axis symmetry. Displacements at the model bottom are constrained in both horizontal and vertical directions, while lateral sides are only constrained in the horizontal direction. Interface elements are assigned around the periphery of the DMW to consider the soil-wall interface roughness and the interface strength can be determined by the strength reduction of the adjacent soils to account for the interface disturbance caused by the wall construction (Jamsawang et al., 2015; Zhang et al., 2024). The total number of elements and nodes of the numerical model are respectively equal to 5062 and 41322.

There are four layers below the ground surface, including a 2.5 m-thick layer of Fill Crust (FC), a 13.5 m-thick layer of Soft to Medium Clay (SMC), a 6 m-thick layer of Stiff Clay (SC), and a 13 m-thick layer of Very Stiff Clay (VSC). The hardening soil model with small strain (HSS) is used to simulate the soil behavior during the excavation phases to account for the stress-strain relationship and small strain stiffness. The soil-wall interface is related to the adjacent soils and is also modelled by the HSS. The DMW is modelled by the linearly elastic perfectly plastic Mohr-Coulomb constitutive model due to its simplicity and efficiency in simulating the basic behavior of cement-treated soils (Ignat et al., 2015; Jamsawang et al., 2015; Oliveira et al., 2011; Phutthananon et al., 2018). The parameters related to the numerical analysis are summarized in Table 1.

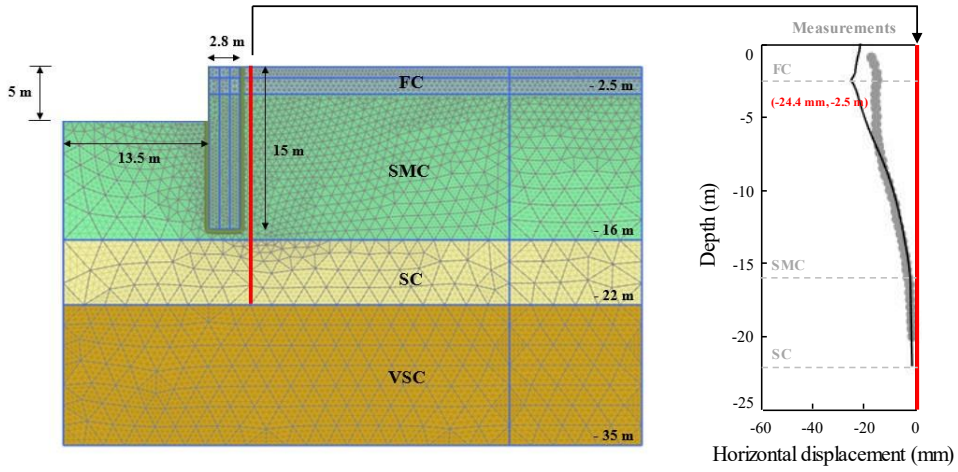

(a) (b)

Fig. 1. DMW-walled excavation (a) FEM model (Waichita et al., 2019) and (b) comparison between the measured and predicted horizontal deflection.

Table 1 Parameters for the numerical simulation (Waichita et al., 2019)

Parameter	Notation (Unit)	Value				
		FC	SMC	SC	VSC	DMW
Material model	-	HSS	HSS	HSS	HSS	MC
Unsaturated unit weight	γ_{dry} (kN/m^3)	17	15	18	18	15
Saturated unit weight	γ_{sat} (kN/m^3)	18	16	19	19	16
Elastic modulus	E (kPa)	-	-	-	-	3.9E5
Secant modulus	E_{50}^{ref} (kPa)	1.5E4	1.3E4	5E4	8E4	-
Oedometer modulus	E_{oed}^{ref} (kPa)	1.5E4	1.3E4	5E4	8E4	-
Unloading/reloading modulus	E_{ur}^{ref} (kPa)	4.5E4	3.9E4	1.5E5	3E5	-
Cohesion	c (kPa)	15	1	15	40	242
Friction angle	φ (°)	27	22	26	26	35
Poisson's ratio	υ_{ur}	0.2	0.2	0.2	0.2	0.2
Over consolidation ratio	OCR	2	1.1	2.5	2.5	1
Power for stress-level dependency of stiffness	m	0.9	0.9	0.9	0.9	-
Reference pressure	p^{ref} (kPa)	100	100	100	100	-
Failure ratio	R_f	0.9	0.9	0.9	0.9	-
Initial shear modulus	G_0^{ref}	1.0E5	7.0E4	1.7E5	3.5E5	-
Reference shear strain	$\gamma_{0.7}$	3E-4	8E-4	3E-4	3E-4	-
Interface	R_{inter}	0.7	0.5	-	-	-

To verify the accuracy of the constructed numerical model, the simulation results are compared with measured data which were collected by an inclinometer tube placed 1 m behind the wall, and the comparisons can be found in Fig. 1. The horizontal deflection profile and the magnitude based on the numerical simulation are generally in good agreement, with the discrepancy remaining within an acceptable

range (Voottipruex et al., 2019). It allows to validate the effectiveness of the numerical evaluations. Besides, it is found that for the numerical simulation, the maximum horizontal displacement is 24.4 mm and occurs at the interface between the layers of FC and SMC. This can be explained by the difference in shear strength (c_{FC} = 15 kPa, φ_{FC} = 27° while c_{SMC} = 1 kPa, φ_{SMC} = 22°) and modulus ($E_{50}^{ref}\_{FC}$ = 1.5E4 kPa and $E_{50}^{ref}\_{SMC}$ = 1.3E4 kPa) of these two layers.

2.2 Optimization design and uncertainty quantification

For a DMW design and construction, the key problem concerned is to ensure adequate safety while keeping the lowest cost. Concerning DMW safety, considerable uncertainty is observed in the soil-cement mixture and the adjacent soil, which is necessary to be accounted for the DMW stability analysis (Fan et al., 2018; Filz and Navin, 2010). It is noted that the DMW-adjacent soil data can be gained before construction and the corresponding uncertainties can be determined during the design phase, thus allowing participation in stability analyses and providing reasonable guidance for DMW design and construction. Conversely, it is not always possible to obtain adequate DMW information before or during construction. Some data can be available after soil-cement mixture hardening, but it is too late to update the design (Fan et al., 2018; Wang et al., 2014a). Therefore, how to design and optimize the DMW with the (DMW and soil) uncertainties consideration while satisfying the safety requirements is essential.

As far as cost is concerned, DMW is primarily affected by the cement content mixed into the soil and the higher the cement content, the higher the cost (Waichita et al., 2019). Besides, the cement content directly affects the value of Unconfined Compressive Strength (UCS), with a strong positive correlation between these two parameters, i.e., the compressive strength gradually increases with increasing cement content (Aiban et al., 1998; Zuo et al., 2023). Consequently, in this study, the UCS of DMW is considered as the design parameter that needs to be optimized with a lower UCS value indicating reduced construction costs. Another reason for considering UCS as the design parameter is that the UCS is widely adopted as the design and construction quality control standard or indicator for soil-cement reinforced excavation (Fan et al., 2018; Han et al., 2002; Wang et al., 2014b; Zhang et al., 2021). In addition, the parameters used in

numerical analyses, i.e., the cohesion and modulus, can be interpreted from the UCS (Porbaha, 1998; Zhang et al., 2021).

Therefore, this study aims to optimize the UCS value to minimize cost while ensuring safety requirements are met, taking into account the uncertainties. It is noted that there is insufficient data available to determine the statistical information of the Bangkok case (Waichita et al., 2019). The uncertainties of the considered random variables are thus derived from existing literature to make the analyses reasonable. A summary of these details is provided in Table 2.

Table 2 Statistical information of parameters with uncertainty consideration

	Parameter	Notation (Unit)	Statistics of parameters			
			Mean value	Coefficient Of Variation (COV)	Range	Distribution
DMW	Unconfined compressive strength	UCS (kPa)	Optimized	0-0.8[a]	50-5000[b]	Log-normal[c]
	E/UCS	R_E	327	0-0.5[d]	20-1000[e]	Log-normal[d]
	c/UCS	R_c	0.2	0-0.5	0.05-0.5[f]	Log-normal
	Friction angle	φ_{DMW} (°)	35	0-0.5	25-43[g]	Log-normal
FC	Secant modulus	${E_{50}}^{ref}{}_{FC}$ (kPa)	1.5E4		-	
	Cohesion	c_{FC} (kPa)	15	0.1[h]	-	Log-normal[h]
	Friction angle	φ_{FC} (°)	27		-	
SMC	Secant modulus	${E_{50}}^{ref}{}_{SMC}$ (kPa)	1.3E4		-	
	Cohesion	c_{SMC} (kPa)	1	0.1[h]	-	Log-normal[h]
	Friction angle	φ_{SMC} (°)	22		-	

Note:
[a] Based on values given by (Chen et al., 2011; Kasama et al., 2012; Pan et al., 2018); [b] (Ayeldeen et al., 2016; Jamsawang et al., 2015); [c] (Zhang et al., 2018); [d] (Phutthananon et al., 2023); [e] (Phutthananon et al., 2023; Tracz et al., 2019); [f] (Wijerathna and Liyanapathirana, 2018; Zhang et al., 2021); [g] (Fan et al., 2018; Yapage et al., 2014); [h] (Kayser and Gajan, 2014).

2.2.1 DMW uncertainties

A lognormal distribution is adopted to model the UCS variability, as Zhang et al. (2018) demonstrated that it fits the data better than a normal distribution and prevents negative values. The UCS variability, represented by the COV, is influenced by complex construction processes, natural in-situ soil variability, and differences in construction techniques and workmanship. Consequently, its value varies across different scenarios, making it essential to assess how different levels of variability impact the optimization results. A

COV range of [0, 0.8] is used to explore its effects on the optimized UCS (Fujii et al., 2004), with a value of 0 indicating constant UCS, meaning the optimization is treated as traditional Deterministic-Based Design Optimization (DBDO) (Das and Das, 2010). The UCS optimization range is set between [50 kPa, 5000 kPa] (Ayeldeen et al., 2016; Jamsawang et al., 2015).

For the modulus and cohesion of DMW, a large number of studies have focused on their interpretation based on UCS (Fan et al., 2018; Wang et al., 2014a; Zhou et al., 2023). To maintain simplicity and generality, a linear relationship is adopted, where the ratios of R_E, Rc are introduced to determine the modulus and cohesion by $E = R_E \times \text{UCS}$, $c = Rc \times \text{UCS}$ (Fan et al., 2018; Szymkiewicz et al., 2015; Wang et al., 2014b). It has been validated that 'considering uncertainty in the ratio R_E instead of assuming a constant value' provides a more realistic representation of the relationship between the modulus and UCS (Phutthananon et al., 2023). Therefore, the uncertainties of interpretation ratios are considered in this study, with a range of [0, 0.5] to allow representing different degrees of variabilities. Additionally, the uncertainty of the friction angle is included, as it is a key parameter in characterizing the shear strength of DMW.

2.2.2 Soil uncertainties

For the soil layers FC and SMC, the uncertainties in strength and stiffness parameters are considered, as the excavation is carried out through these two layers. A total of six soil parameters, including the cohesion, friction angle and modulus for both the FC and SMC layers, are modeled as random variables following a lognormal distribution. Additionally, due to the lack of sufficient data and for the sake of simplicity and conservative design, the input parameters are assumed to be statistically independent (Greco, 2016).

3. PCK-assisted RBDO

The reliability-based design optimization is carried out to solve the UCS optimization and its performance is presented in this section. The limit state function is first introduced, which is followed by the Polynomial Chaos Kriging-assisted double-loop approach for the RBDO analysis. Two loops, including

an outer loop (constrained (1+1)-CMA-ES) for design parameter optimization and an inner loop (PCK-Monte Carlo Simulation (MCS)) for reliability analysis, iteratively update the design parameter (UCS) to meet the safety target level and reliability constraints. The automatic procedure is then detailed by a flowchart.

3.1 Limit state function

For stability analysis with uncertainty consideration, the limit state function should be determined to check whether the DMW is safe or not. The maximum wall deflection and the ground surface settlement are important criteria to assess the potential damages caused by excavations (Luo et al., 2011), and the wall deflection is considered as the criterion in this study since (i) excessive wall deflection may cause severe damage to adjacent structures and utilities (Kung et al., 2007), (ii) a well-established relationship exists between horizontal wall deflection and ground surface settlement (Zhang et al., 2024), indicating that when wall deflection meets the required criteria, ground surface settlement typically remains within acceptable limits, and (iii) wall deflection is relatively easier to measure in practical engineering compared to the ground surface settlement, and it is widely used in a lot of standards, codes and publications (Philipponnat and Hubert, 2016; Zhang et al., 2024). The limit state function $G(\boldsymbol{x})$ can be defined by:

$$G(\boldsymbol{x})=\delta_{hm}-\delta_{hm\_lim} \tag{1}$$

where $\boldsymbol{x}$ denotes the vector of variables, δ_{hm} is the wall deflection calculated by the numerical simulation, δ_{hm_lim} is the limiting maximum wall deflection and its determination depends on the standard, project, soil type, excavation depth and the construction method. It can be referred to codes, manuals and the available researches. In this study, a $\delta_{hm\_lim}=2\%H$ is used for the limiting maximum wall deflection which is suggested in the existing studies (Fok et al., 2012; Marr and Hawkes, 2010; Wang et al., 2010). Eq. (1) defines the failure modes associated with the serviceability limit state (SLS), where excavation is considered safe when $G(X) \leq 0$, and failure occurs when $G(X) > 0$.

3.2 Inner loop: PCK-MCS

The active learning method PCK-MCS is carried out for the inner loop reliability analysis, the PCK is constructed as a surrogate model and then the MCS is performed to provide the failure probability P_f. The automatic procedure can be found in the pseudo-algorithm presented in **Algorithm 1** and the details are described below.

Algorithm 1: PCK-MCS

Input: random variables
Output: failure probability

1.1 Generate initial samples based on the statistical information using LHS.
1.2 Compute the relevant outputs (maximum wall deflection) based on Section 2.1.
1.3 PCK surrogate model construction.
(a) build a PCK surrogate model based on the initial input-output datasets and PCK theory (Eq. (2));
(b) *criterion 1*: check that the leave-one-out error (Eq. (3)) is less than the threshold value, if it does, go to Step 1.3(c), otherwise, go to Step 1.3(d);
(c) *criterion 2*: generate a large number of samples and check whether the number of the predictions in the failure domain meets the criterion (Eq. (5)), if it does, go to Step 1.4, otherwise, go to Step 1.3(d);
(d) enrich the datasets with the 'best' next input-output to improve the PCK surrogate model. The input is selected based on the ***U*** learning function as shown in Eq. (4). Go back to Step 1.3(a).
1.4 Perform MCS to determine the failure probability as shown in Eq. (6).

The initial Experimental Design (ED) can be generated by the Latin Hypercube Sampling (LHS), which is widely used for the sample generation by the fact that it combines the advantages of traditional random sampling and stratified sampling (Helton and Davis, 2003). Then the output (the maximum wall deflection) can be determined based on the deterministic models as shown in Section 2.1. The initial PCK surrogate model can then be constructed according to the PCK theory (Marelli and Sudret, 2014), which can be expressed as:

$$Y \approx M^{PCK}(\boldsymbol{x}) = \sum_{i \in A} \alpha_i \Phi_i(\boldsymbol{x}) + \sigma^2 Z(\boldsymbol{x}) \tag{2}$$

where $M^{PCK}(\boldsymbol{x})$ is the model output approximation using PCK and A is the index set of polynomials. $\sum_{i \in A} \alpha_i \Phi_i(\boldsymbol{x})$ is the sum of orthonormal polynomials used to characterize the trend in the universal Kriging formula. Its construction involves determining the multivariate polynomial basis $\Phi_i(\boldsymbol{x})$ (i.e., the tensor product of univariate orthonormal polynomials), and the corresponding unknown coefficients α_i (estimated by the least-square minimization method) (Pan et al., 2020). σ^2 and $Z(\boldsymbol{x})$ represent the variance and the

zero mean unit variance stationary Gaussian process defined by an autocorrelation function (Matern-5/2 model used in this study) between two sample points $R(|x-x'|;\theta)$, where θ is the hyper-parameter to be estimated (Marelli and Sudret, 2014).

To ensure the accuracy of the PCK surrogate model, two criteria are set and one of them is the Leave-One-Out error Err_{LOO}, which is defined by:

$$Err_{LOO} = \frac{1}{N}\left[\frac{\sum_{i=1}^{N}(Y^{(i)} - \mu_{y,(-i)}(x^{(i)}))^2}{\mathrm{Var}(Y)}\right] \leq Err_{LOO\_\mathrm{tar.}} \tag{3}$$

where $\mu_{y,(-i)}(x^{(i)})$ is the prediction values based on the PCK surrogate model using all the experimental design points except $x^{(i)}$, $Y^{(i)}$ is the exact model response, and Var(Y) is the corresponding estimated variance. The surrogate model can be considered qualified when the Err_{LOO} value is smaller than the target value Err_{LOO_tar}. If it does not satisfy, the enrichment of the ED should be performed by the $\boldsymbol{U}$ function expressed by (Moustapha et al., 2022):

$$U(x_l) = \frac{|\mu_M(x_l)|}{\sigma_M(x_l)}, l \in N_{MCS} \tag{4}$$

where $\mu_M(x_l)$ and $\sigma_M(x_l)$ are respectively the mean and standard deviation of the model output at sample x_l. The newly added sample is selected from the candidate pool (N_{MCS} samples used for the MCS calculation as shown in Eq. (6)) by minimizing Eq. (4), i.e., $S_n = \arg\min U$, which identifies the points with the highest likelihood being misclassified as failed or safe.

If the surrogate model meets the criterion as shown in Eq. (3), a large number of samples are generated by the LHS and are predicted by the PCK surrogate model. Another criterion, which is related to the prediction size in the failure domain, is proposed and can be defined as:

$$Err_{N_f} = \frac{N_f^{(k-1)} - N_f^{(k)}}{N_f^{(k-1)}} \leq Err_{N_{f\_\mathrm{tar.}}} \tag{5}$$

where $N_f^{(k)}$ and $N_f^{(k-1)}$ are respectively the number of failed samples at the *k*-th and ($k-1$)-th enrichment iterations, and $Err_{N_f\_\text{tar.}}$ is the threshold value for this criterion. For robustness, the PCK construction can be stopped only after 10 consecutive iterations satisfy this criterion (Eq. (5)). Otherwise, the experimental design should be enriched as shown in Eq. (4).

After the surrogate model construction, the traditional reliability methods can be carried out. In this study, the crudest simulation method: MCS is performed and the failure probability can be determined by (Phoon and Ching, 2015):

$$P_f = \frac{1}{N_{MCS}} \sum_{k=1}^{N_{MCS}} I_k \tag{6}$$

where N_{MCS} is the total number of samples, and based on the constructed PCK surrogate model, predictions are made for all samples, yielding N_{MCS} corresponding values of $G(x)$. The indicator function I_k is equal to 1 when the failure occurs, i.e., $I_k(G(x)>0)=1$, otherwise, the value of I_k is set to 0.

3.3 Outer loop: Constrained (1+1)-CMA-ES

The outer loop of RBDO is regarded as an optimization problem, which is to determine the optimal values subject to the specified constraints, i.e.,

$$\boldsymbol{x}^* = \arg\min_{\boldsymbol{x}_d \in \boldsymbol{D}} g(\boldsymbol{x}_d) \quad \text{subject to: } f_j(\boldsymbol{x}_d) \le 0,\ j = 1,\ldots, m$$

where $\boldsymbol{x}_d$ represents the vector of the optimized design parameters, and $\boldsymbol{D}$ denotes the search space defined by the lower and upper bounds of these parameters, $\boldsymbol{x}^*$ is the optimal solution, *g* is the objective function, *f* is constraint functions that need to be fulfilled and *m* (>0) is the number of constraint functions (Marelli and Sudret, 2014).

The constrained (1+1)-CMA-ES is introduced and performed in this study to solve the optimization problem. It is an evolutionary optimization algorithm and a variant of the well-known Covariance Matrix Adaptation-Evolution Strategy (CMA-ES) algorithm in which one parent generates exactly one offspring

and takes into account optimization constraints (Arnold and Hansen, 2012). The analysis procedure of the constrained (1+1)-CMA-ES is depicted in **Algorithm 2** and the details are described below.

Algorithm 2: Constrained (1+1)-CMA-ES

Input: design parameter search space, objective function, constraints
Output: optimized design parameter

2.1 Initialize the parameters of the algorithm, including the initial value of design variables (the mean value of upper and lower bounds), global step size σ, Cholesky decomposition A, and exponentially fading record v_j.
2.2 Optimize the design variables by an iterative process.
(a) generate an offspring candidate solution $x_{da}{}^{t}$ based on Eq. (7);
(b) evaluate the constraints at the offspring candidate $f_j(x_{da}{}^{t})$. If $f_j(x_{da}{}^{t}) \le 0$, go to Step 2.2(c). Otherwise, update the exponentially fading record v_j based on Eq. (8) and Cholesky factor **A** based on Eq. (9), and go back to Step 2.2(a);
(c) evaluate the objective function $g(x_{da}{}^{t})$, and update the success probability estimate P_{succ} (Eq. (10)) and global step size σ (Eq. (11)). Check whether $g(x_{da}{}^{t}) \le g(x_{db})$, if it does, replace x_{db} with $x_{da}{}^{t}$, and update the search path $\boldsymbol{s}$ and Cholesky factor **A** based on Eqs. (12)-(15), then go to Step 2.3. Otherwise, i.e., if $g(x_{da}{}^{t}) > g(x_{db})$, go to Step 2.2(d);
(d) check $x_{da}{}^{t}$ is worse than its fifth ancestor, if it is, update **A** according to Eqs. (16) and (17), and go back to Step 2.2(a). Otherwise, go back to Step 2.2(a) directly with the updated P_{succ} (Eq. (10)) and σ (Eq. (11)).
2.3 Check convergence criterion, i.e., whether the global step size is smaller than the threshold. If it is, output the optimized value. Otherwise, return to Step 2.2.

The optimization is an iterative process, and the offspring candidate solution at t^{th} iteration $x_{da}{}^{t}$ can be determined by:

$$x_{da}{}^{t} = x_{db} + \sigma \mathbf{A}\mathbf{z} \tag{7}$$

where x_{db} is the parent solution for each iteration, σ is the global step size of the strategy, **z** is a vector of standard normal distributions and provides the randomness of the algorithm, and **A** is the Cholesky decomposition which is decomposed from positive definite covariance matrix **C** (i.e., $\mathbf{C} = \mathbf{A}\mathbf{A}^{\mathrm{T}}$) that is used to express the relationships of the design variables. Cholesky decomposition **A** is directly used in the optimization instead of the covariance matrix **C**, to avoid computationally expensive matrix decomposition and allow for easy updates during the optimization process (Arnold and Hansen, 2010). The Cholesky decomposition **A** is initialized to be a $n \times n$ identity matrix, where n is the number of the design parameters.

The offspring candidate solution is then checked to satisfy the constraints, i.e., $f_j(x_{da}{}^{t}) \le 0$. If the j^{th} constraint is violated, the exponentially fading record v_j, which is to reduce variances of offspring candidate

solutions along the normal vectors of constraint boundaries near the parent solution, is updated according to:

$$v_j \leftarrow (1-a)v_j + a\mathbf{A}\mathbf{z} \tag{8}$$

where parameter $a \in (0, 1)$ determines how quickly the information present in the constraint vectors fades, and is often determined by $1/(n+2)$, and the initial v_j is 0.

Besides, the Cholesky factor of the covariance matrix **A** should also be updated according to:

$$\mathbf{A} \leftarrow \mathbf{A} - \frac{\beta}{\sum_{j=1}^{m} \mathbf{I}_{f_j(x_{da}{}^t)>0}} \sum_{j=1}^{m} \mathbf{I}_{f_j(x_{da}{}^t)>0} \frac{v_j w_j^{\mathrm{T}}}{w_j^{\mathrm{T}} w_j} \tag{9}$$

where $w_j = A^{-1}v_j$ and $\mathbf{I}_{f_j(x_{da}{}^t)>0}$ equals 1 if $f_j(x_{da}{}^t)>0$ and 0 otherwise. Parameter β controls the size of the updates and is often determined by $0.1/(n+2)$. Substitute updated **A** into Eq. (7) and update new offspring solution $x_{da}{}^t$.

Conversely, if the offspring respects the constraint requirements, i.e., $\sum_{j=1}^{m} \mathbf{I}_{f_j(x_{da}{}^t)>0} = 0$, the objective function $g(x)$ should be evaluated and the success probability estimation P_{succ} and the global step size σ can be updated by:

$$P_{\mathrm{succ}} \leftarrow (1-b)P_{\mathrm{succ}} + b\mathbf{I}_{(g(x_{da}{}^t)<g(x_{db}))} \tag{10}$$

$$\sigma \leftarrow \sigma \exp\left(\frac{1}{c}\frac{P_{\mathrm{succ}} - P_{\mathrm{target}}}{1-P_{\mathrm{succ}}}\right) \tag{11}$$

where $\mathbf{I}_{(g(x_{da}{}^t)<g(x_{db}))}$ is an indicator function and should be 1 if $g(x_{da}{}^t)>g(x_{db})$, otherwise it should be 0. The parameters b and c control the updates and are set as $1/12$ and $1+n/2$, respectively.

If $g(x_{da}{}^t) \le g(x_{db})$, x_{db} can be replaced by $x_{da}{}^t$ and then update the search path $\boldsymbol{s}$ and the Cholesky factor **A**:

$$\boldsymbol{s} \leftarrow (1-d)\boldsymbol{s} + \sqrt{d(2-d)}\mathbf{A}\mathbf{z} \tag{12}$$

$$\mathbf{A} \leftarrow e\mathbf{A} + h\boldsymbol{s}\boldsymbol{w}^{\mathrm{T}} \tag{13}$$

where d is determined by $2/(n+2)$ and $\boldsymbol{w}$ is set to $\mathbf{A}^{-1}\boldsymbol{s}$. e and h can be defined by:

$$e = \sqrt{1-c_{\mathrm{cov}}^{+}} \tag{14}$$

$$h = \frac{\sqrt{1-c_{\text{cov}}^{+}}}{\|\boldsymbol{w}\|^2}\left(\sqrt{1+\frac{c_{\text{cov}}^{+}}{1-c_{\text{cov}}^{+}}\|\boldsymbol{w}\|^2}-1\right) \tag{15}$$

where c_{cov}^{+} can be determined by $2/(n^2+6)$.

Conversely, if $g(x_{da}{}^{t})>g(x_{db})$, and $x_{da}{}^{t}$ is worse than its fifth order ancestor, i.e., $g(x_{da}{}^{t}) \le g(x_{da}{}^{t-4})$, the Cholesky factor **A** should be updated by Eq. (13) with the coefficients *e* and *h* as below:

$$e = \sqrt{1-c_{\text{cov}}^{-}} \tag{16}$$

$$h = \frac{\sqrt{1-c_{\text{cov}}^{-}}}{\|\mathbf{z}\|^2}\left(\sqrt{1+\frac{c_{\text{cov}}^{-}}{1-c_{\text{cov}}^{-}}\|\mathbf{z}\|^2}-1\right) \tag{17}$$

where c_{cov}^{-} can be determined by $c_{\text{cov}}^{-} = \min\left(\frac{0.4}{n^{1.6}+1}, \frac{1}{2\|\mathbf{z}\|^2-1}\right)$.

The iteration of the optimization procedure will be carried out until the criteria are satisfied with the requirements. In this study, the global step size is considered and should meet $\sigma<\sigma_{\text{tar}}$, i.e., the algorithm stops if the value of σ becomes smaller than the threshold σ_{tar}.

3.4 Procedure of PCK-RBDO-ES

This procedure includes the inner loop to construct the PCK surrogate model and to provide the failure probability based on the MCS, and the outer loop Constrained (1+1)-CMA-ES to optimize the required UCS. The procedure is presented by a flowchart in Fig. 2 to provide a comprehensive understanding of the proposed framework, which are detailed below:

Step 1: **Preparation**. Construct the deterministic models (as presented in Section 2.1); Determine the design & environmental parameters and the relevant statistical information (i.e., the distribution, mean value and coefficient of variation as presented in Section 2.2). It is noted that the design parameter of the DMW refers to the UCS, while the others (i.e., layer FC: $E_{50}{}^{\text{ref}}{}_{\text{FC}}$, c_{FC}, φ_{FC}; layer SMC: $E_{50}{}^{\text{ref}}{}_{\text{SMC}}$, c_{SMC}, φ_{SMC}; DMW: φ_{DMW}, R_c, R_E) are the environmental variables.

Step 2: **Optimization model formulation**. The optimization model formulation includes the determination of the objective functions, design variables and constraints. The objective function is determined based on

the optimization purpose (Section 2.2); The hard constraint determination is related to the limit state function as shown in Section 3.1 and the failure probability computation as described in Eq. (6).

Step 3: **PCK surrogate model construction**. An iterative algorithm and an adaptive sampling technique are used for the PCK surrogate model construction as shown in Section 3.2. It is noted that it is time-consuming to construct a local PCK surrogate model at each design parameter optimization, particularly for the case that the optimization requires many iterations to converge. Therefore, an augmented reliability space is introduced to cover all nested reliability analyses, which covers both design and environmental variables at once. The necessary experimental designs cover uniformly this augmented space in order to make the limit-state surfaces accurate wherever they may be evaluated during the optimization process (Dubourg et al., 2011). The augmented space can be defined as a hypercube which involves the design variables $\mathbf{R}$ and environmental variables $\mathbf{Z}$, and can be expressed by the tensor product $\mathbf{R} \times \mathbf{Z}$. In more details, the design variables $\mathbf{R}$ can be defined by:

$$\mathbf{R} = \prod_{t=1}^{T} [q_{d_t}^{-}, q_{d_t}^{+}] \tag{18}$$

where $q_{dt}^{-} = F_{x_t|d_t^{-}}^{-1}(\alpha_{d_t}/2)$ and $q_{dt}^{+} = F_{x_t|d_t^{+}}^{-1}(1-\alpha_{d_t}/2)$. $F_{x_t|d_t^{-}}^{-1}$ and $F_{x_t|d_t^{+}}^{-1}$ are the inverse cumulative distribution functions of the design variables at the extreme lower bound d_t^{-} and upper bound d_t^{+} of the design space. α_{d_t} is the probability of sampling outside the augmented space in the t^{th} dimension.

For the environmental variables, the hypercube can be defined according to the distributions. Once the augmented space is determined, the samples can be generated based on the LHS, which is followed by the surrogate model construction presented in Section 3.2.

Step 4: **Design optimization**. The constrained (1+1)-CMA-ES is carried out to explore the optimized design parameter through multiple iterations until the global step size meets the requirements as shown in Section 3.3.

For the PCK surrogate model construction, the convergence criteria $Err_{LOO\_tar.}$ and $Err_{N_f\_tar.}$ are set to 0.02 respectively (Zhang et al., 2024). For the constrained (1+1)-CMA-ES, the threshold for the global step length is defined as 0.001 (Marelli and Sudret, 2014). The script for automatic modelling is coded in Matlab (2022), Python and Plaxis 2D (2022), where Plaxis 2D is mainly carried out for the wall deflection calculations, and Matlab & Python are used for the pre- and post-processing of the PCK-RBDO-ES analysis to achieve a totally automatic process.

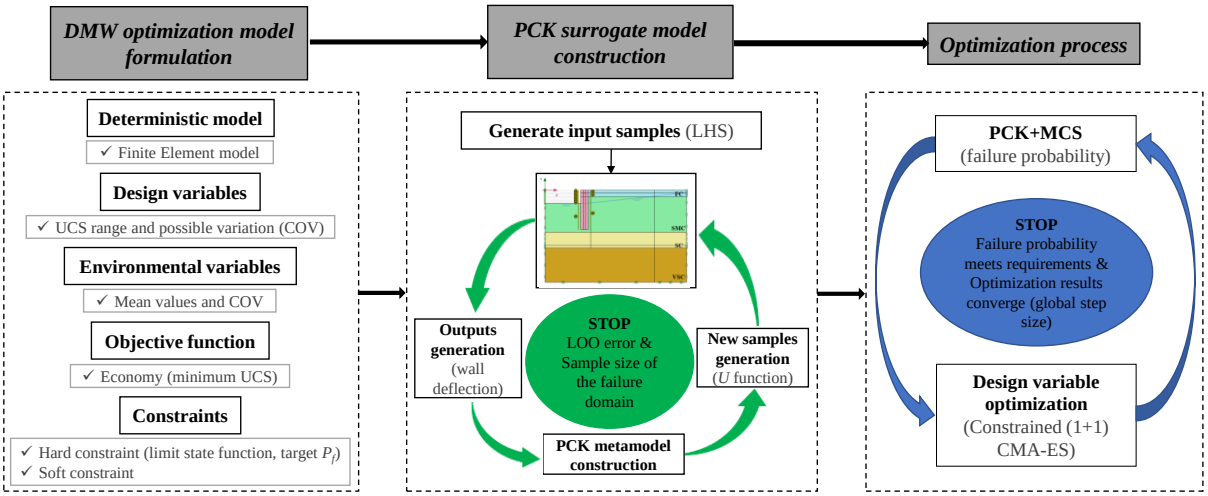

Fig. 2. Flowchart of the RBDO analysis.

4. Results and validation

For the design of the DMW, the objective is to achieve the required reliability level with the minimum UCS, and the RBDO problem for the DMW can be described as:

$$\begin{aligned} &\text{minimize } g(\boldsymbol{x}_d, \boldsymbol{x}_e) = \text{UCS} \\ &\text{subject to } \mathrm{P}(G(\boldsymbol{x}_d, \boldsymbol{x}_e) \le 0) \le P_{f\_\text{target}} \\ &\boldsymbol{x}_d^{-} \le \boldsymbol{x}_d \le \boldsymbol{x}_d^{+} \end{aligned}$$

where $\boldsymbol{x}_e$ is the vector of the environmental variables (i.e., layer FC: ${E_{50}}^{\text{ref}}_{\text{FC}}$, c_{FC}, φ_{FC}; layer SMC: ${E_{50}}^{\text{ref}}_{\text{SMC}}$, c_{SMC}, φ_{SMC}; DMW: φ_{DMW}, R_c, R_E), P_{f_target} is the targeted failure probability and it is recommended in a range of [0.011, 0.097] for the Serviceability Limit State problems (Lü et al., 2017). $\boldsymbol{x}_d^{-}$ and $\boldsymbol{x}_d^{+}$ are the lower and upper limits of the design variable, i.e., UCS.

4.1 Optimization results

The PCK-RBDO-ES procedure described in Section 3.4 is carried out. The statistical information can be found in Table 2 and for the reference case, the COVs for all environmental variables are set to 0.1 and the COV of design variable is assumed to be 0.5. The target failure probability is considered as 0.06.

The optimization procedure starts with the construction of the PCK surrogate model, which aims to replace the time-consuming numerical simulations. Firstly, 50 initial samples are generated, which is followed by the sample enrichment and the process can be found in Figs. 3(a) and (b). It is found that after 27 enrichments, the Err_{LOO} satisfies the requirements (Eq. (3)) whereas the failure sample size for a large number of samples prediction (100,000 samples for each prediction) is highly variable. Accordingly, more samples are generated into the experimental design used for the surrogate model construction, and the Err_{N_f} is continuously smaller than the threshold value (Eq. (5)) from the 63rd enrichment and the subsequent ten iterations. Therefore, a total of 123 samples, which include 50 initial samples and 73 enrichments, are used for the PCK surrogate model construction.

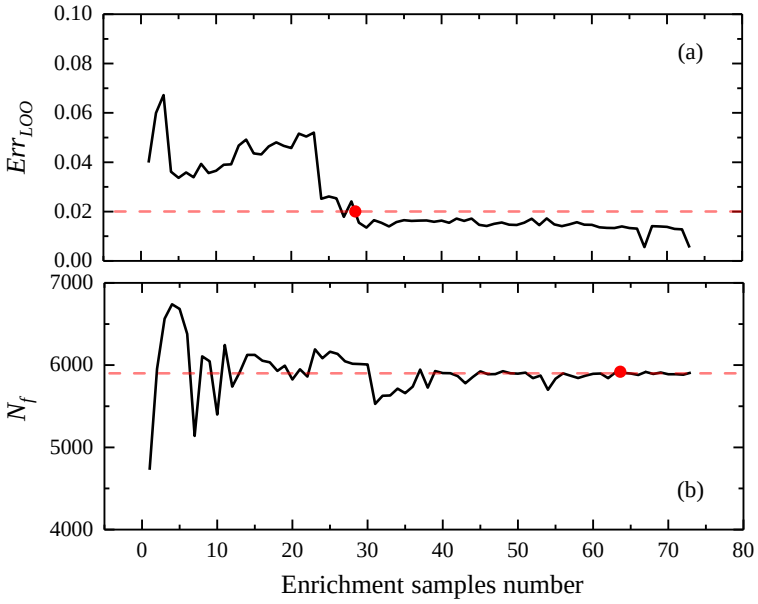

Fig. 3. Surrogate model construction process with (a) Err_{LOO} convergence and (b) Err_{Nf} convergence.

The constrained (1+1)-CMA-ES is followed to be carried out and the optimization procedure can be found in Fig. 4. Fig. 4(a) depicts the convergence process of the global step size σ and it is noted that σ is

started from 1650 since the default initial value of σ is one-third of the difference between the upper and lower bounds (Marelli and Sudret, 2014). The σ value is decreased with the iteration and the optimization is stopped after 573 iterations as the value of σ is smaller than 0.001. Correspondingly, the optimized UCS value for each iteration is also given in Fig. 4(b), and it can be found that the UCS value varies greatly in the first 100 iterations, and then the UCS value gradually converges and remains basically unchanged after 150 iterations, with a convergence value of 1492 kPa. In consequence, considering the uncertainties in the (soil and DMW) parameters, the DMW needs a UCS of 1492 kPa to satisfy the target failure probability requirement of 0.06.

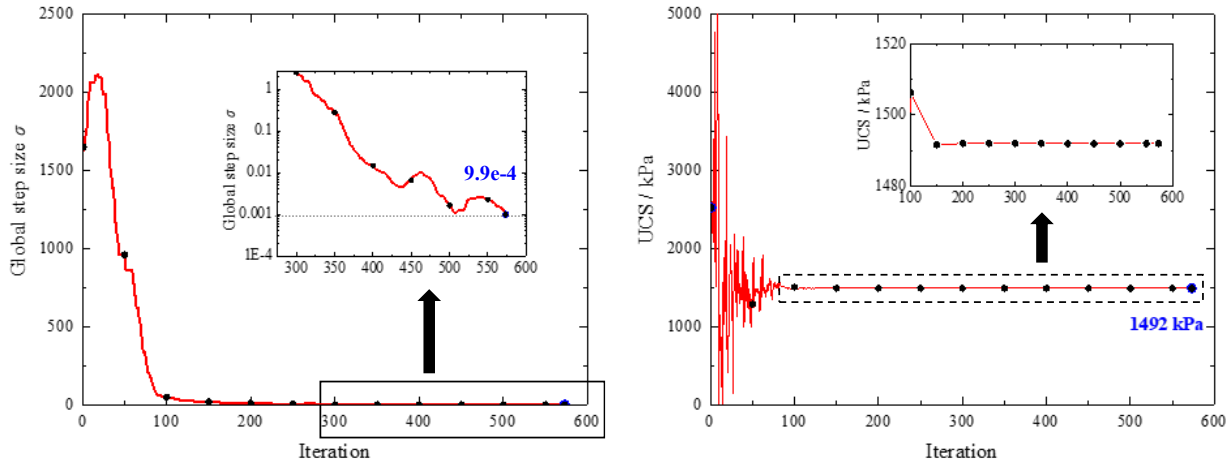

Fig. 4. Optimization process of constrained (1+1)-CMA-ES with (a) Global step size and (b) UCS.

4.2 PCK-RBDO-ES validation

A total of 123 deterministic simulations are required for the PCK surrogate model construction and a UCS of 1492 kPa is provided for the DMW design and construction. The optimization accuracy may be examined by comparing the results obtained from the direct double-loop analysis (i.e., without the PCK surrogate model assistance). However, it is important to note that the direct double-loop analysis is time-consuming and unaffordable, as it requires about 57,300,000 simulations for the same number of iterations and optimal design (573 iterative optimization loops and for each iteration, 100,000 deterministic simulations are performed for the failure probability determination). To address this issue, the procedure accuracy is discussed in terms of (i) the validation of the PCK surrogate model evaluations. If the maximum

wall deflections obtained from the PCK surrogate model can be correctly predicted and classified (i.e., whether there is a failure or a safety), then the subsequent optimization procedure can be implemented in a correct manner; (ii) the reliability analysis based on the optimized UCS. If the obtained failure probability is equal to the target failure probability of 0.06, the optimized UCS value is accurate. The validation details are provided in Section 4.2.1 and Section 4.2.2.

In addition, the existing optimization methods (such as the RIA and PMA methodologies), are significantly affected by the initial value of design variable during the optimization (i.e., different initial values of UCS lead to different optimized results), which are defined by the designers and therefore heavily dependent on the designer's previous experience (Lü et al., 2017). In this study, the effects of the initial values on the optimization results based on the constrained (1+1)-CMA-ES are also investigated and can be found in Section 4.2.3.

4.2.1 PCK validation

The PCK surrogate model is validated in this section and the comparisons are presented in Fig. 5. A total of 500 samples are generated using the LHS based on the statistical information of the variables, specifically the UCS samples are generated uniformly over the range of [50 kPa, 5000 kPa] while the other parameters are randomly generated according to a lognormal distribution. Fig. 5(a) depicts the maximum wall deflection comparisons between the PCK surrogate model predictions and the numerical simulations. It is observed that the maximum wall deflection could be divided into three regions, including Region 1: [0, 60 mm], Region 2: (60 mm, 140 mm], and Region 3: (140 mm, 300 mm]. Among the three regions, the prediction results in Region 2 perform better than the others, with points distributed on the diagonal and within the range of ±5% error lines, which implies that the PCK surrogate model can provide δ_{hm} similar to the numerical simulations. However, the differences between the PCK predictions and the numerical simulations in Region 1 and Region 3 are relatively larger, with some points being distributed outside the ± 5% error lines (whereas most of them are within ±20% error bounds).

The reasons for these discrepancies can be explained by the fact that (i) compared to Region 1 and Region 2, the extreme cases with large horizontal displacements of Region 3 are fewer generated by the LHS due to the given statistical characteristics of the random variables, and thus the predictive performance in this region is poor; (ii) the limiting maximum wall deflection is set to 100 mm and the enrichments generated by the ***U*** function are mainly the samples with the highest probability of being misclassified as failure or safe. Therefore, the added samples are those with the calculated maximum wall deflection around 100 mm, which can improve the prediction accuracy around the region of δ_{hm} = 100 mm and check whether the samples are safe or not, i.e., the predicted δ_{hm} is less than or greater than 100 mm. Then, the failure probability can be calculated accurately based on the failed sample number to the total sample number, which ensures the accuracy of the subsequent optimization. The relevant classification in Region 2 can be found in Fig. 5(b), and it is noted that the safe and failed samples determined by PCK and FEM are almost the same, which ensures the accuracy of the prediction and classification. In other regions (Regions 1 and 3), the δ_{hm} values in Region 1 are in the range of [0, 60 mm], which are much smaller than 100 mm, while the δ_{hm} values in Region 3 are far larger than 100 mm. The points in these two regions can thus be easily classified as safe or failure, even though there are some discrepancies between the PCK predictions and the numerical simulation results. As a result, the requirements for prediction accuracy in Regions 1 and 3 are not as stringent as in Region 2.

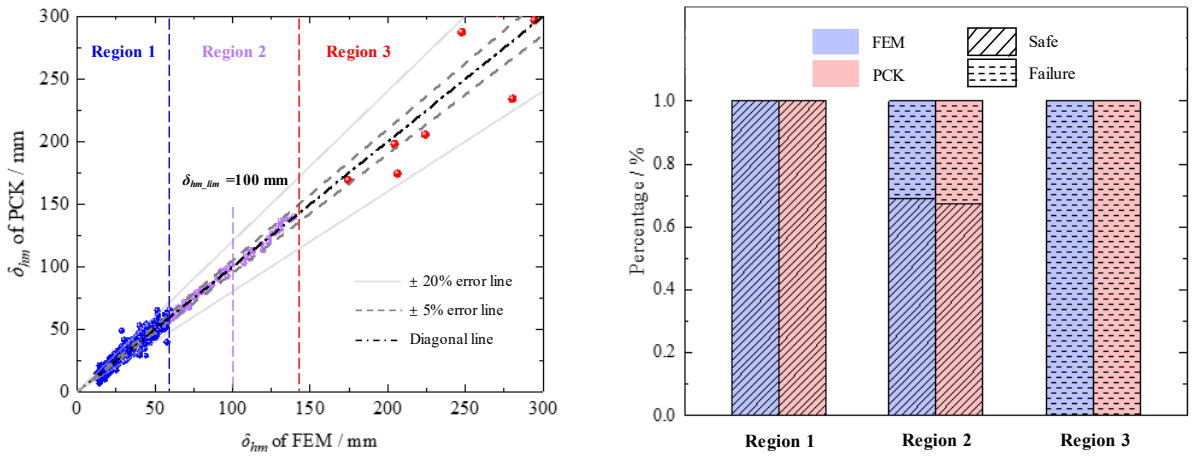

(a) (b)

Fig. 5. PCK surrogate model verification of (a) δ_{hm} comparison and (b) Safe / Failure classification.

4.2.2 Forward reliability verification

The reliability analysis is performed based on the optimized UCS: 1492 kPa with a COV of 0.5 and a lognormal distribution, while the other parameters are the same with the reference case. The MSFEM analysis procedure proposed by Zhang et al. (2024) is implemented in this study to determine the failure probability, distributions (PDF: probability density function, CDF: cumulative distribution function) and the statistical moments (mean value and standard deviation) of the maximum wall deflections. The results are summarized in Fig. 6 and it is found that δ_{hm} is widely distributed in the range of [0, 400 mm], with 5954 samples out of a total of 100,000 samples having δ_{hm} greater than 100 mm. A failure probability of 0.06 is then provided, which is consistent with the target failure probability. It demonstrates the optimized 1492 kPa is accurate and verifies the validity of the optimization.

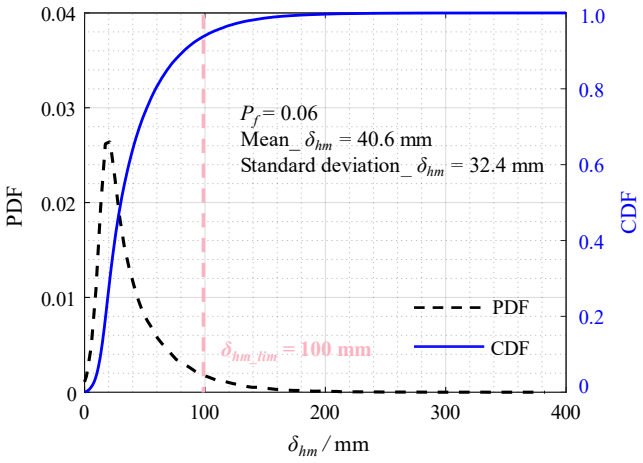

Fig. 6. PDF, CDF and statistical moments of δ_{hm}.

4.2.3 Optimization stability

The optimization is investigated for different initial values, and the optimization process (variation of the global step size σ and the optimized UCS) is shown in Fig. 7. The default initial value of constrained (1+1)-CMA-ES is the average of the upper and lower bounds i.e., 2525 kPa (Marelli and Sudret, 2014). After 573 iterations, the iteration is stopped with a σ of 9.9e-4 and provides a UCS of 1492 kPa as detailed in Section 4.1 (Fig. 7(a)). For comparison, three other initial values are discussed, including 2000 kPa, 3000 kPa and 4000 kPa, and the results are shown in Figs. 7(b), 7(c) and 7(d), respectively. It can be seen that optimized UCS converges to 1492 kPa after several iterations (437, 581 and 383 iterations, respectively),

regardless of the initial values. It verifies that the constrained (1+1)-CMA-ES is robust and independent of the optimized initial values, which is more accurate and flexible.

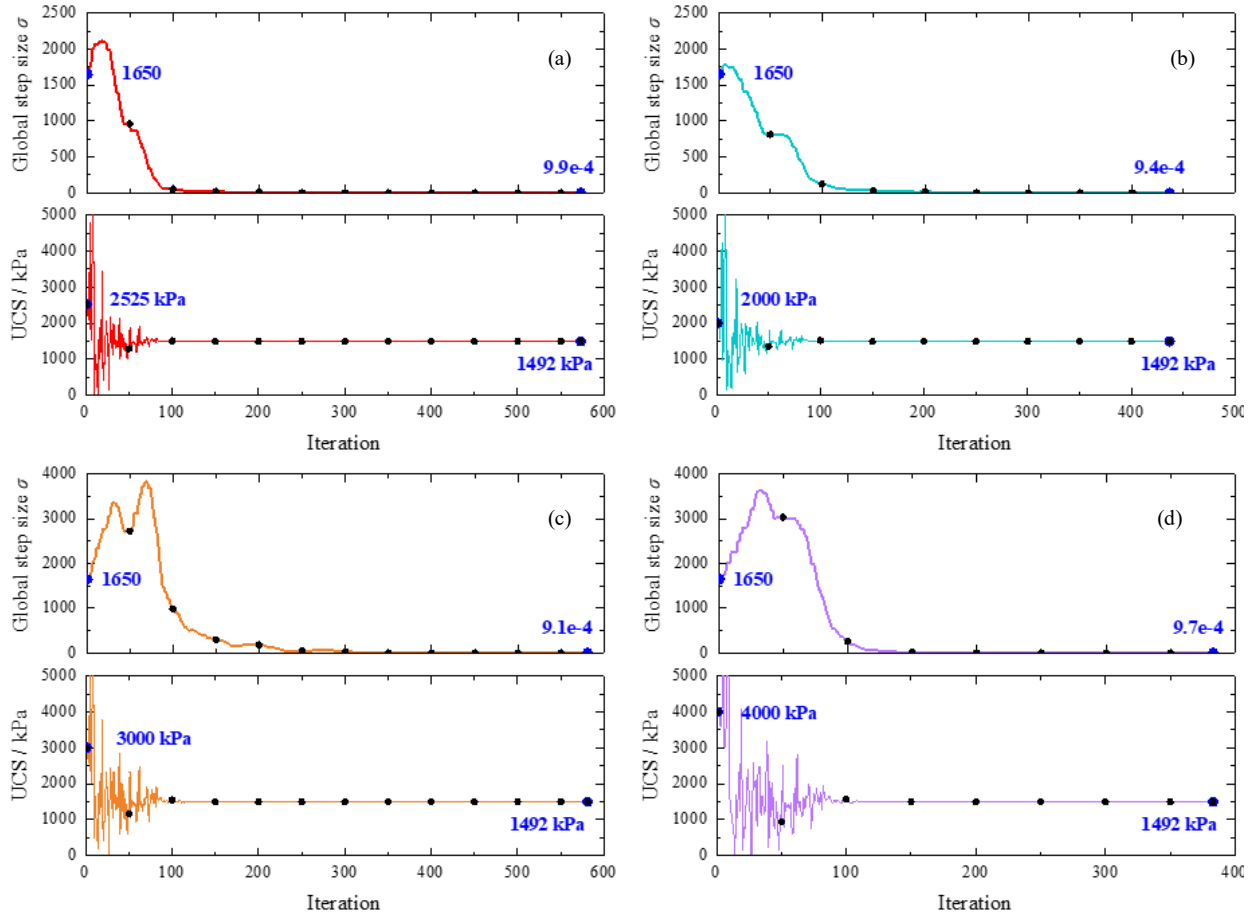

Fig. 7. Optimization for different initial designs (a) Initial value = 2525 kPa, (b) Initial value = 2000 kPa, (c) Initial value = 3000 kPa and (d) Initial value = 4000 kPa.

4.3 Efficiency survey

It is noted that the proposed PCK-RBDO-ES only needs around 123 numerical evaluations for the PCK surrogate model construction. The subsequent optimization is based on the PCK, which spends several minutes and is negligible compared to the direct double-loop approach that would have required 57,300,000 simulations. The efficiency relies on the active-learning surrogate model construction and the selection of the important samples (i.e., the samples with the calculated δ_{hm} being around 100 mm). For example, Region 2 of Fig. 5 is important and the prediction accuracy must be ensured, whereas Regions 1 and 3 are not so demanding because they are all far away from the limiting values and can be easily classified.

In summary, this study offers an automated method for determining the required UCS, taking into account the potential uncertainties in DMW and surrounding soils, along with the target reliability level of the DMW system, to balance the trade-off between cost-effectiveness and safety. All of the above discussions ensure the accuracy and efficiency of the proposed PCK-RBDO-ES. Benefiting from its advantages, several discussions are carried out and more details can be found in Section 5.

5. Discussion and remarks

Three aspects are investigated in this section, including the effects of DMW uncertainty, adjacent soil uncertainty, and target reliability requirements on the UCS optimization. It should be noted that all parameters are consistent with the reference case, otherwise the modified parameters are mentioned.

5.1 DMW uncertainty consideration

DMW uncertainty may be influenced by construction process, natural variability of in-situ soils, or potential measurement errors. In order to better understand the impact of DMW uncertainty on optimized UCS, different COV values of the DMW-related variables (i.e., UCS, cohesion R_c, modulus R_E and friction angle φ_{DMW}) are discussed and the results are presented in Fig. 8. The COV of UCS takes values in a range of [0, 0.8] and a value of 0 indicates that the optimized UCS is constant without considering uncertainty in which case the optimization problem can be regarded as the traditional DBDO (Das and Das, 2010). Different COV sets for R_c, R_E and φ_{DMW} are provided for comparison.

It is noted that the uncertainty plays a significant role in UCS prediction. With the increase of the COV_UCS, the optimized UCS also increases, and the difference in predicted UCS becomes larger as the uncertainties in R_c, R_E and φ_{DMW} increase. For example, when COV_UCS is equal to 0.8 and the COV value is 0.1 for R_c, R_E and φ_{DMW}, the required UCS increases by about 855 kPa compared to the DBDO case, while the difference can be up to 1669 kPa when the COV values of R_c, R_E and φ_{DMW} are increased to 0.5. Therefore, it is important to consider the uncertainty in UCS for the DMW design and construction, otherwise the DBDO results cannot support the DMW stability due to the significant difference. Besides, the uncertainties

in cohesion, modulus and friction angle have a great effect on the UCS prediction and it is more essential to consider the UCS uncertainty when the COVs of the R_c, R_E and φ_{DMW} are significant.

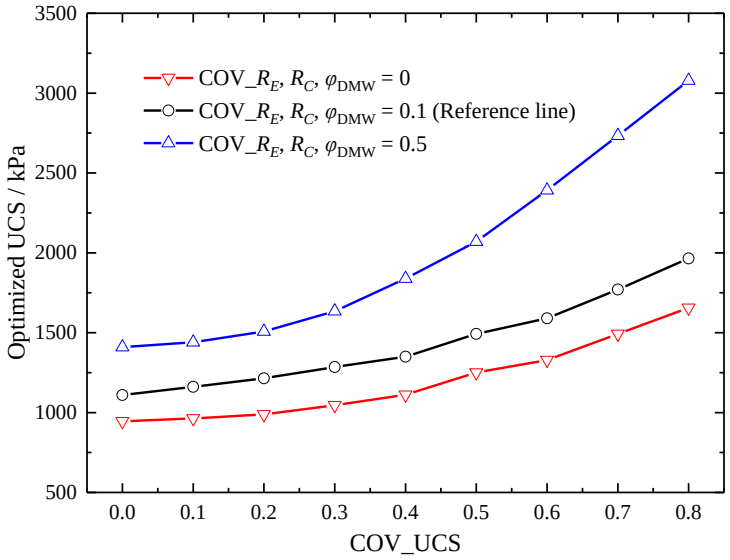

Fig. 8. Effects of DMW uncertainties.

Sensitivity analysis of DMW-related variables is also investigated and the results are presented in Fig. 9. Taking COV_R_c, R_E, φ_{DMW} = 0 as the base case, one DMW-related parameter uncertainty effect on the predicted UCS is discussed with a coefficient of variation of 0.5, while keeping COV of the other two parameters equal to 0. The results show that the DMW stiffness parameter (modulus) uncertainty consideration is more significant compared to the strength parameters' (cohesion and friction angle). This is because the stiffness affects wall deformations and displacements, which are critical for the serviceability analysis, while the strength parameters primarily influence the ultimate load capacity. For the strength parameters, the COV of friction angle on the obtained optimal UCS is almost negligible since the results are essentially consistent with the base case results that not uncertainty consideration. It indicates that the variation of the friction angle has less influence on the DMW stability. It is similar to the existing studies, which demonstrated that the cohesion is the main index affecting the strength of cement soil instead of the friction angle (Zhang et al., 2021).

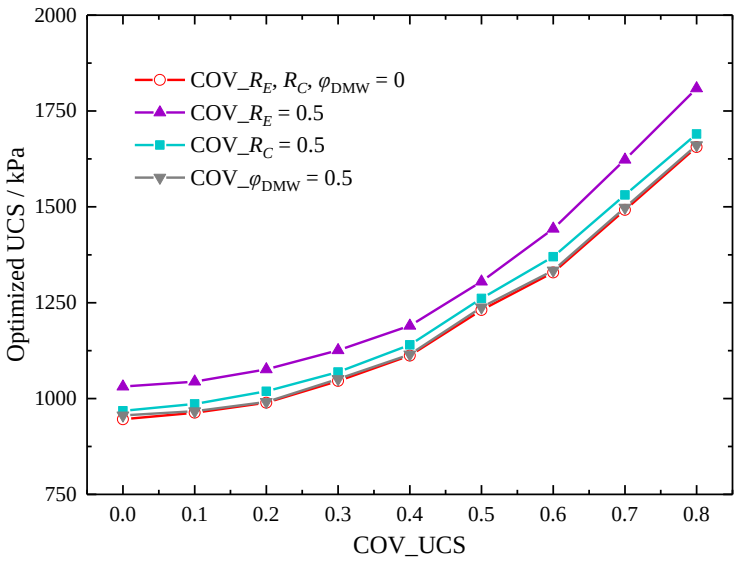

Fig. 9. Sensitivity analysis of DMW uncertainties.

In general, the uncertainties associated with DMW parameters, especially modulus and cohesion, should be carefully considered and determined. In addition, reducing the level of uncertainty in the DMW parameters can reduce the required UCS and further decrease the construction costs (Zuo et al., 2023). This can be achieved through careful quality control and effective construction management. For example, stringent quality control measures are implemented during construction to ensure that the construction materials and workmanship comply with the specified standards.

5.2 Soil uncertainty consideration

It is noted that the soil uncertainties also play significant roles in the DMW stability, therefore, 'how soil uncertainties affect the UCS optimization' and 'which layer and which parameter is more important for the UCS optimization' are essential to be investigated. The effects of soil parameter uncertainties in layers FC and SMC (as shown in Fig. 1) on the UCS optimization are respectively discussed and presented in Figs. 10 and 11. Taking the case without soil uncertainty consideration (i.e., COV_ $E_{50}{}^{ref}{}_{FC}$, c_{FC}, φ_{FC}, $E_{50}{}^{ref}{}_{SMC}$, c_{SMC}, φ_{SMC} = 0) as the base case, the effect of uncertainty in one soil-related parameter on the predicted UCS is then discussed with the coefficient of variation being 0.1, while the other soil-related parameters are constant.

There is no doubt that the required UCS increases as the uncertainty in soil parameters increases, and different parameters and soil layers show different effects on the predicted UCS. In layer FC, the cohesion contributes the most, which is followed by the friction angle and the modulus. For layer SMC, the friction angle is more important whereas the cohesion and the modulus do not change significantly the required UCS. Compared to layer FC, layer SMC has a greater impact on the results. Taking COV_UCS being 0.5 as an example, when uncertainties in modulus, cohesion, and friction angle are taken into account, the UCS differences for the FC layer compared to the base case are 2 kPa, 32 kPa, and 7 kPa, respectively, while the UCS differences for the SMC layer are 19 kPa, 6 kPa, and 282 kPa. This can be explained by the fact that the layer SMC (13.5 m) is much thicker than the layer FC (2.5 m) and most of the DMW construction took place in SMC layer (12.5 m out of 15 m).

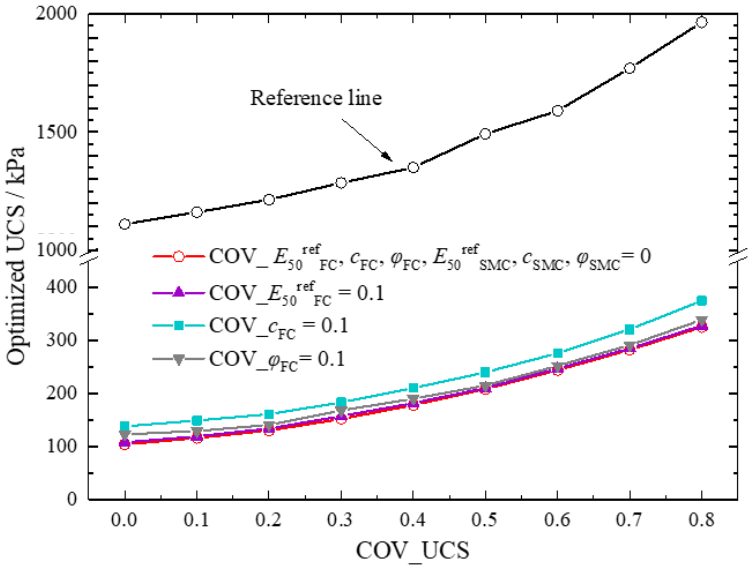

Fig. 10. Effects of the soil uncertainties in layer FC.

Besides, the friction angle of the SMC layer is the most important among the soil variables as it impacts significantly the optimized UCS, especially when COV_UCS is 0.8, with a difference reaching up to 514 kPa compared to the base case. Therefore, more attention should be paid to the friction angle of layer SMC during sampling and measurement phases to obtain more accurate statistical information. In addition, compared to the reference line (i.e., the COVs of all environmental variables are 0.1), the difference in optimized UCS with and without all soil uncertainties (as depicted in Figs. 10 and 11) is more significant

than the difference observed when DMW uncertainties are not considered (as presented in Fig. 8). This can be explained by the fact that there are six soil parameters considered as the random variables while the DMW only has three environmental variables. This also highlights the importance of the soil uncertainty consideration.

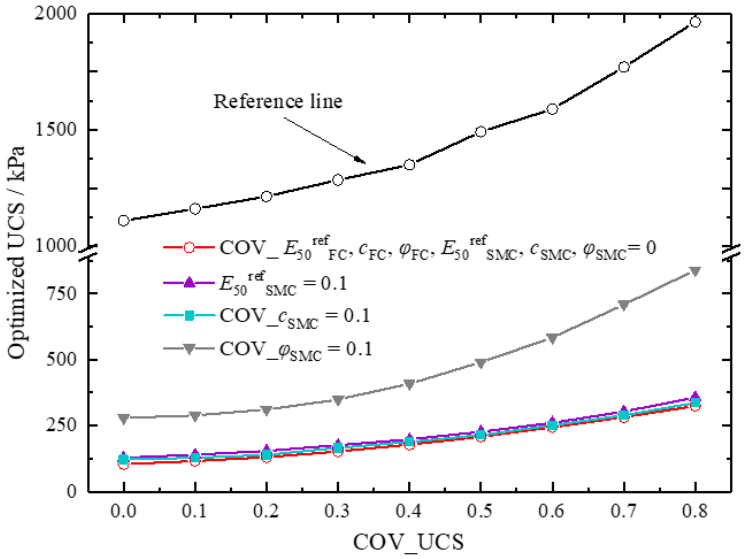

Fig. 11. Effects of the soil uncertainties in layer SMC.

5.3 Influence of target reliability requirement

The above studies are based on a target failure probability of 0.06. However, it is noted that the target P_f is not definitive and its determination changes with the project details, local standards, experiences and knowledge of practitioners, or failure types (Liu and Cheung, 2020; Lü et al., 2017). For example, the recommended P_f is in the range of [0.011, 0.097] for the SLS, while for the Ultimate Limit State (ULS), the target P_f ranges from 1.3e-6 to 9.7e-4 (CEN, 2007; JCSS, 2001; Lenner et al., 2019).

This section discusses the impact of the target failure probability on the RBDO results, with the target P_f ranging from 0.011 to 0.097 due to the displacement-based criterion implementation. The results are presented in Fig. 12. There is no doubt that the increased target failure probability leads to a decrease in UCS since the safety requirements are reduced. The required UCS is changed less with the target safety level when the target P_f is greater than 0.07, whereas its variation becomes significant when the target P_f is smaller than 0.07. For example, the UCS difference is 45 kPa when the target P_f varies from 0.08 to 0.07

(COV_UCS = 0), while the difference is 779 kPa when the target P_f varies from 0.07 to 0.06, and when the target P_f decreases to 0.05, the difference can be up to 3500 kPa. In such case, the increase of the UCS is not obvious to improve the DMW stability, and using other structural supports or reinforcements may be more effective (Nishanthan et al., 2018). The results are similar to the findings of Jamsawang et al. (2015), they showed that the modulus plays a significant role in the wall deflection reduction when its value is small, whereas the wall deflection remains approximately constant in the range of higher modulus values.

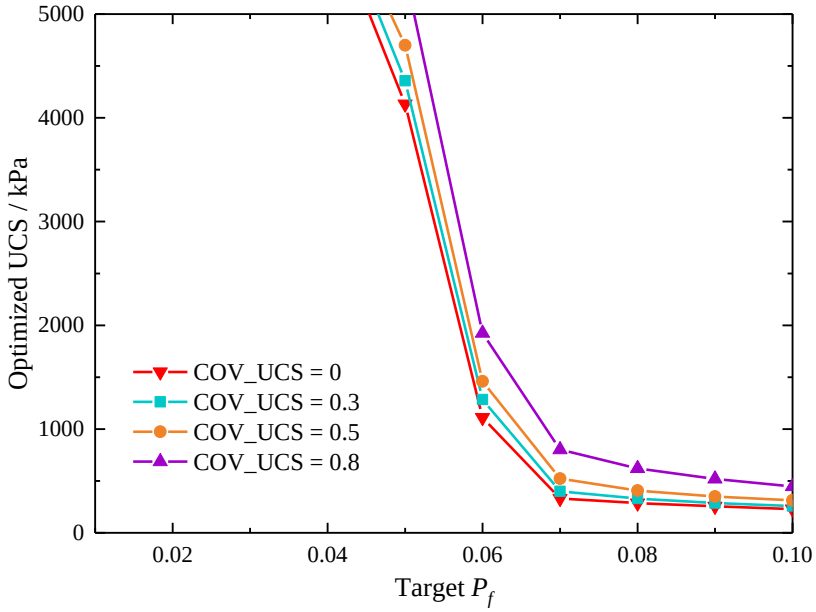

Fig. 12. Influence of the target failure probability on the optimal UCS values.

Besides, the required UCS difference is increased as COV_UCS increases. For example, the difference is up to 1123 kPa when the target P_f varies from 0.07 to 0.06 with a COV_UCS being 0.8, whereas the difference value is 779 kPa when the COV_UCS is 0. The importance of the uncertainty reduction during DMW construction is highlighted again. In addition, the UCS is not sufficient to meet the required safety level if the target P_f is small (such as the $P_f < 0.045$), which means that a suitable target reliability index is required to ensure the successful implementation of the RBDO, otherwise, an optimal design cannot be found. In such case, more supports should be installed to satisfy the safety requirements.

This section demonstrates the importance of the target reliability level determination, and provides some insights for similar projects based on the design figures.

5.4 Practical implementation and extension of the proposed procedure

This study can automatically provide the required UCS with consideration of the potential DMW uncertainty and adjacent soil uncertainty, as well as the target reliability level of the DMW system to address the trade-off between economy and safety. The targeted approach of constructing specific PCK metamodels for individual cases offers improved computational efficiency and practical applicability, enabling faster optimization and more effective solutions to real-world engineering problems. Looking forward, a promising prospect is the adoption of reliability-based optimal design method PCK-RBDO-ES in more DMWs and other geotechnical structures (such as slopes, tunnels and embankments) to incorporate the potential uncertainties and costs during design and construction, ensuring stable operation and long-term sustainability.

It is noted that the RBDO problem formulation is dependent on the specific cases, i.e., the identification of the environmental and design variables, and their statistical information, the deterministic model, the objective function, and the constraints, are different for different cases, which should be determined based on the project details (Hu et al., 2023; Lü et al., 2017; Zhang and Ji, 2022). Particularly for the uncertainty determination, it is noted that different COV values significantly affect the optimized UCS, and both of the COV of design and environmental variables are important as discussed in Section 5.1 and Section 5.2. Therefore, careful attention must be given to data collection and statistical analysis. Another concern is the deterministic model construction, a 2D numerical model is used in this study to predict the maximum wall deflection. However, it can also be achieved through analytical methods if they can give reasonable results or 3D numerical simulations if the problem cannot be simplified into a 2D model. Additionally, the choice of constitutive models for the DMW should be project-specific. If higher accuracy is required and the relevant parameters can be precisely determined, more advanced models such as the Hardening Soil model or HSS could be used.

Once the RBDO problem is formulated, the metamodel construction and optimization process of the proposed procedure PCK-RBDO-ES as outlined in Section 4.3, can be applied to optimize the design

parameters. It should be noted that the reliability method PCK-MCS is carried out in this study for the failure probability calculation. However, for cases involving very small failure probabilities (less than 10^{-5}), standard MCS may be insufficient due to the large size of required samples. In such cases, the Subset Simulation offers a viable alternative, as it reduces the variance of the MCS estimator while requiring fewer evaluations, thus offering a more efficient approach for estimating failure probabilities (Zhang, 2023).

6. Conclusions

An efficient PCK-assisted RBDO procedure: PCK-RBDO-ES is proposed to optimize the Deep Mixing Wall design and construction with consideration of the potential uncertainties, safety requirements and costs. An automatic PCK-based MCS is carried out for the reliability analysis in the inner loop, and the constrained (1+1)-CMA-ES is performed to do the optimization in the outer loop. Some conclusions are summarized below:

1) The proposed PCK-RBDO-ES is effective in providing the required UCS that takes into account the parameters uncertainties and meets the predefined performance requirements. Compared to the existing RBDO methods, the sample-wised automatic PCK construction can reduce the required numerical simulations, and the constrained (1+1)-CMA-ES is more robust and can provide stable results even with different initial values. This makes it suitable for adoption in a wider range of DMWs as well as other geotechnical structures, such as slopes, tunnels and embankments.

2) DMW uncertainties are very important and should be considered during design and construction, particularly the UCS, modulus and cohesion. The resulted optimal design of UCS increased with the increase of uncertainty level, therefore, a standardized construction would be beneficial in decreasing DMW uncertainty and further reducing DMW construction costs.

3) For the studied case, uncertainties of soil parameters play significant roles in the UCS optimization, particularly the thick layer SMC. The soil parameters importance ranking is also given, and the friction angle of layer SMC and cohesion of layer FC are more important and should be cautious during data

collection and variability modelling, to provide more accurate statistical information. Conversely, the insignificant parameters can be considered as deterministic, which can reduce the collection work, simplify the numerical models and reduce the computational effort.

4) The target safety requirement is essential to the UCS determination. Higher requirements lead to higher UCS and the increased UCS cannot significantly increase the DMW stability when the target P_f is smaller than 0.06 and other supports are suggested to be installed.

This study provides a robust framework and rational option for the design and construction of DMWs in urban excavation projects, ultimately contributing to more resilient and efficient underground infrastructure development. There are still aspects that need to be improved in future research: (i) the properties of cement-treated soils using deep mixing technique tend to be highly variable in their spatial distribution, i.e., different strengths and stiffnesses at different locations. It is one of the main uncertainties affecting the performance of geotechnical systems (Pittaro and Mace, 2024). The spatial variability simulation is more complex, while provides a more realistic representation, which will be conducted to investigate its effect on DMW stability; (ii) the PCK employed in this study enhances the computational efficiency. However, it becomes less effective for high-dimensional problems, particularly when the number of random variables exceeds 20 (Moustapha et al., 2022), such as in large-scale problems with numerous random variables or cases involving random fields. Improving the efficiency of surrogate model construction for high-dimensional problems is crucial; (iii) this study provides the required UCS for the safe DMW construction, and the UCS is affected by several factors, such as the cement content, cement/water ratio, and the curing conditions (Mojtahedi et al., 2023). It is interesting to optimize and provide more specific values for these parameters so that more practical suggestions for the DMW construction can be provided.

Acknowledgements

The authors thank gratefully the “Franki Foundations” for the financial support.

References

Aiban, S.A., Al-Abdul Wahhab, H.I., Al-Amoudi, O.S.B., Ahmed, H.R., 1998. Performance of a stabilized marl base: A case study. Construction and Building Materials 12, 329–340. https://doi.org/10.1016/S0950-0618(98)00023-3

Arnold, D., Hansen, N., 2012. A (1 + 1) - CMA - ES for Constrained Optimisation, in: Proceedings of the 14th Annual Conference on Genetic and Evolutionary Computation. pp. 297–304. https://doi.org/https://inria.hal.science/hal-00696268

Arnold, D. V., Hansen, N., 2010. Active covariance matrix adaptation for the (1+ 1)-CMA-ES, in: 12th Annual Conference on Genetic and Evolutionary Computation. pp. 385–392.

Ayeldeen, M., Hara, Y., Kitazume, M., Negm, A., 2016. Unconfined compressive strength of compacted disturbed cement-stabilized soft clay. International Journal of Geosynthetics and Ground Engineering 1–10.

CEN, 2007. Eurocode - Basis of structural design (EN 1990). Brussels.

Chen, J., Lee, F.H., Ng, C.C., 2011. Statistical analysis for strength variation of deep mixing columns in Singapore, in: Geo-Frontiers 2011: Advances in Geotechnical Engineering. pp. 576–584.

Das, M.R., Das, S.K., 2010. Reliability Based Optimum Design of Sheet Pile Wall Using a Simple Optimization Tool, in: Indian Geotechnical Conference. Mumbai, India.

Denies, N., Huybrechts, N., 2017. Deep mixing method for the construction of earth and water retaining walls. RILEM Technical Letters 2, 1–9. https://doi.org/10.21809/rilemtechlett.2017.27

Denies, N., Vervoort, A., Huybrechts, N., 2012. Soil mix walls as retaining structures,Belgian practice, in: TC211 International Symposium on Ground Improvement IS-GI. pp. 83–97.

Dubourg, V., Sudret, B., Bourinet, J.M., 2011. Reliability-based design optimization using kriging surrogates and subset simulation. Structural and Multidisciplinary Optimization 44, 673–690. https://doi.org/10.1007/s00158-011-0653-8

Fan, J., Wang, D., Qian, D., 2018. Soil-cement mixture properties and design considerations for reinforced excavation. Journal of Rock Mechanics and Geotechnical Engineering 10, 791–797. https://doi.org/10.1016/j.jrmge.2018.03.004

Filz, G.M., Navin, M.P., 2010. A practical method to account for strength variability of deep-mixed ground, in: GeoFlorida 2010: Advances in Analysis, Modeling & Design. pp. 2426–2433.

Fok, P., Neo, B., Veeresh, C., Wen, D., Goh, K., 2012. Limiting values of retaining wall displacements and impact to the adjacent structures. The IES Journal Part A: Civil & Structural Engineering 5, 134–139. https://doi.org/https://doi.org/10.1080/19373260.2012.696447

Fujii, M., Kawamura, M., Tamura, M., Watanabe, K., Mizoguchi, E., 2004. Quality evaluation method for soil-cement column by deep mixing method. Journal of the Society of Materials Science, Japan 53, 9–12.

Greco, V.R., 2016. Variability and correlation of strength parameters inferred from direct shear tests. Geotechnical and Geological Engineering 34, 585–603.

Guo, X., Dias, D., 2020. Kriging based reliability and sensitivity analysis – Application to the stability of an earth dam. Computers and Geotechnics 120, 103411. https://doi.org/10.1016/j.compgeo.2019.103411

Guo, X., Du, D., Dias, D., 2019. Reliability analysis of tunnel lining considering soil spatial variability. Engineering Structures 196. https://doi.org/10.1016/j.engstruct.2019.109332

Han, J., Zhou, H.T., Ye, F., 2002. State-of-practice review of deep soil mixing techniques in China. Transportation Research Record 49–57. https://doi.org/10.3141/1808-06

Helton, J.C., Davis, F.J., 2003. Latin hypercube sampling and the propagation of uncertainty in analyses of complex systems. Reliability Engineering and System Safety 81, 23–69. https://doi.org/10.1007/3-540-54029-6_187

Hoy, M., Srijaroen, C., Horpibulsuk, S., Phunpeng, V., Rachan, R., Arulrajah, A., 2023. Innovative solution: soil cement column walls as a temporary retaining structure for excavation in soft Bangkok clay. Smart Construction and Sustainable Cities 1, 1–19. https://doi.org/10.1007/s44268-023-00017-z

Hu, Y., Ji, J., Sun, Z., Dias, D., 2023. First order reliability-based design optimization of 3D pile-reinforced slopes with Pareto optimality. Computers and Geotechnics 162, 105635. https://doi.org/10.1016/j.compgeo.2023.105635

Huang, Y., He, Z., Yashima, A., Chen, Z., Li, C., 2022. Multi-objective optimization design of pile-anchor structures for slopes based on reliability theory considering the spatial variability of soil properties. Computers and Geotechnics 147, 104751. https://doi.org/10.1016/j.compgeo.2022.104751

Ignat, R., Baker, S., Larsson, S., Liedberg, S., 2015. Two- and three-dimensional analyses of excavation support with rows of dry deep mixing columns. Computers and Geotechnics 66, 16–30. https://doi.org/10.1016/j.compgeo.2015.01.011

Jamsawang, P., Jamnam, S., Jongpradist, P., Tanseng, P., Horpibulsuk, S., 2017. Numerical analysis of lateral movements and strut forces in deep cement mixing walls with top-down construction in soft clay. Computers and Geotechnics 88, 174–181. https://doi.org/10.1016/j.compgeo.2017.03.018

Jamsawang, P., Voottipruex, P., Jongpradist, P., Bergado, D.T., 2015. Parameters affecting the lateral movements of compound deep cement mixing walls by numerical simulations and parametric analyses. Acta Geotechnica 10, 797–812. https://doi.org/10.1007/s11440-015-0417-5

Jamsawang, P., Voottipruex, P., Tanseng, P., Jongpradist, P., Bergado, D.T., 2019. Effectiveness of deep cement mixing walls with top-down construction for deep excavations in soft clay: case study and 3D simulation. Acta Geotechnica 14, 225–246. https://doi.org/10.1007/s11440-018-0660-7

JCSS, 2001. Probabilistic model code. Joint Committee on Structural Safety.

Kasama, K., Whittle, A.J., Zen, K., 2012. Effect of spatial variability on the bearing capacity of cement-treated ground. Soils and Foundations 52, 600–619. https://doi.org/10.1016/j.sandf.2012.07.003

Kayser, M., Gajan, S., 2014. Application of probabilistic methods to characterize soil variability and their effects on bearing capacity and settlement of shallow foundations: state of the art. International Journal of Geotechnical Engineering. International Journal of Geotechnical Engineering 8, 352–364.

Khorramian, K., Alhashmi, A.E., Oudah, F., 2023. Optimized active learning Kriging reliability based assessment of laterally loaded pile groups modeled using random finite element analysis. Computers and Geotechnics 154, 105135. https://doi.org/10.1016/j.compgeo.2022.105135

Kung, G.T., Juang, C.H., Hsiao, E.C., Hashash, Y.M., 2007. Simplified Model for Wall Deflection and Ground-Surface Settlement Caused by Braced Excavation in Clays Simplified Model for Wall Deflection and Ground-Surface Settlement Caused by Braced Excavation in Clays. Journal of Geotechnical and Geoenvironmental Engineering 0241. https://doi.org/10.1061/(ASCE)1090-0241(2007)133

Larsson, S., Bergman, N., 2015. Probabilistic design of dry deep mixing using an observational approach. Proceedings of the Institution of Civil Engineers: Ground Improvement 168, 300–311. https://doi.org/10.1680/grim.14.00011

Lenner, R., Viljoen, C., van Nierop, S., 2019. A comparative study of target reliability index derivation for reinforced concrete structures governed by serviceability limit state. Structural Concrete 20, 670–677. https://doi.org/10.1002/suco.201800202

Li, C., Zhou, J., Armaghani, D.J., Cao, W., Yagiz, S., 2021. Stochastic assessment of hard rock pillar stability based on the geological strength index system. Geomechanics and Geophysics for Geo-Energy and Geo-Resources 7, 1–24. https://doi.org/10.1007/s40948-021-00243-8

Liu, W.S., Cheung, S.H., 2020. Decoupled reliability-based geotechnical design of deep excavations of soil with spatial variability. Applied Mathematical Modelling 85, 46–59. https://doi.org/10.1016/j.apm.2020.04.001

Liu, X., Liu, Y., Li, X., Yang, Z., Jiang, S.H., 2023. Efficient adaptive reliability-based design optimization for geotechnical structures with multiple design parameters. Computers and Geotechnics 162, 105675. https://doi.org/10.1016/j.compgeo.2023.105675

Lü, Q., Xiao, Z.P., Ji, J., Zheng, J., 2017. Reliability based design optimization for a rock tunnel support system with multiple failure modes using response surface method. Tunnelling and Underground Space Technology 70, 1–10. https://doi.org/10.1016/j.tust.2017.06.017

Luo, Z., Atamturktur, S., Juang, C.H., Huang, H., Lin, P., 2011. Probability of serviceability failure in a braced excavation in a spatially random field : Fuzzy finite element approach. Computers and Geotechnics 38, 1031–1040. https://doi.org/10.1016/j.compgeo.2011.07.009

Man, J., Zhang, T., Huang, H., Dias, D., 2023. Probabilistic analysis of tunnel face seismic stability in layered rock masses using polynomial Chaos Kriging metamodel. Jo`urnal of Rock Mechanics and Geotechnical Engineering. https://doi.org/10.1016/j.jrmge.2023.09.020

Marelli, S., Sudret, B., 2014. UQLab: A framework for Uncertainty Quantification in MATLAB. Vulnerability, Uncertainty, Risk ©ASCE 2554–2563.

Marr, W.A., Hawkes, M., 2010. Displacement-based design for deep excavations, in: Earth Retention Conference 3. pp. 82–100.

MATLAB, 2022. MATLAB version: 9.12.0 (R2022a), Natick, Massachusetts: The MathWorks Inc.; 2022.

Mojtahedi, F., Ahmadihosseini, A., Sadeghi, H., 2023. An artificial intelligence based data-driven method for forecasting unconfined compressive strength of cement stabilized soil by deep mixing technique. Geotechnical and Geological Engineering 41, 491–514. https://doi.org/https://doi.org/10.1007/s10706-022-02297-1

Moustapha, M., Marelli, S., Sudret, B., 2022. Active learning for structural reliability: Survey, general framework and benchmark. Structural Safety 96, 102174. https://doi.org/10.1016/j.strusafe.2021.102174
Moustapha, M., Sudret, B., 2019. Surrogate-assisted reliability-based design optimization: a survey and a new general framework. Structural and Multidisciplinary Optimization 60, 2157–2176. https://doi.org/https://doi.org/10.48550/arXiv.1901.03311
Nishanthan, R., Liyanapathirana, D.S., Leo, C.J., 2018. Deep Cement Mixed Walls with Steel Inclusions for Excavation Support. Geotechnical and Geological Engineering 36, 3375–3389. https://doi.org/https://doi.org/10.1007/s10706-018-0539-2
Okoro, A., Khan, F., Ahmed, S., 2023. Dependency effect on the reliability-based design optimization of complex offshore structure. Reliability Engineering and System Safety 231, 109026. https://doi.org/10.1016/j.ress.2022.109026
Oliveira, P.J. V., Pinheiro, J.L., Correia, A.A., 2011. Numerical analysis of an embankment built on soft soil reinforced with deep mixing columns: Parametric study. Computers and Geotechnics 38, 566–576.
Pan, Q., Qu, X., Liu, L., Dias, D., 2020. A sequential sparse polynomial chaos expansion using Bayesian regression for geotechnical reliability estimations. International Journal for Numerical and Analytical Methods in Geomechanics 44, 874–889. https://doi.org/10.1002/nag.3044
Pan, Y., Shi, G., Liu, Y., Lee, F.., 2018. Effect of spatial variability on performance of cement-treated soil slab during deep excavation. Construction and Building Materials 505–519.
Peixoto, A., Sousa, E., Gomes, P., 2012. Permanent excavation support in urban area using cutter soil mixing technology at Cannes, France, in: International Symposium of ISSMGE-TC211. Recent Research, Advances & Execution Aspects of Ground Improvement Works. pp. 233–242.
Philipponnat, G., Hubert, B., 2016. Fondations et ouvrages en terre. Eyrolles.
Phoon, K.K., Ching, J., 2015. Risk and reliability in geotechnical engineering, CRC Press. ed. Boca Raton.
Phutthananon, C., Jongpradist, P., Kandavorawong, K., Dias, D., Guo, X., Jamsawang, P., 2023. Reliability assessment for serviceability limit states of stiffened deep cement mixing column-supported embankments. Journal of Rock Mechanics and Geotechnical Engineering 15, 2402–2422. https://doi.org/10.1016/j.jrmge.2023.05.008
Phutthananon, C., Jongpradist, P., Yensri, P., Jamsawang, P., 2018. Dependence of ultimate bearing capacity and failure behavior of T-shaped deep cement mixing piles on enlarged cap shape and pile strength. Computers and Geotechnics 97, 27–41. https://doi.org/10.1016/j.compgeo.2017.12.013
Pittaro, G.A., Mace, N., 2024. Spatial variability for Deep Cement Mixing in Kallang formation in Singapore. Review of scale of fluctuation and its influence in design. Geotechnical Aspects of Underground Construction in Soft Ground 480–487. https://doi.org/10.1201/9781003413790-57
PLAXIS 2D. (2022). version 2022 update 2. Delft, Netherlands: Bentley Systems Inc., n.d.
Porbaha, A., 1998. State of the art in deep mixing technology: part I. Basic concepts and overview., in: Proceedings of the Institution of Civil Engineers-Ground Improvement. pp. 81–92.
Qu, P., Zhang, L., Zhu, Q., Wu, M., 2023. Probabilistic reliability assessment of twin tunnels considering fluid–solid coupling with physics-guided machine learning. Reliability Engineering & System Safety 231, 109028.
Shao, Y., Macari, E.J., Cai, W., 2005. Compound Deep Soil Mixing Columns for Retaining Structures in Excavations. Journal of Geotechnical and Geoenvironmental Engineering 131, 1370–1377. https://doi.org/10.1061/(asce)1090-0241(2005)131:11(1370)
Spross, J., Bergman, N., Larsson, S., 2021. Reliability-based verification of serviceability limit states of dry deep mixing columns. Journal of Geotechnical and Geoenvironmental Engineering 147, 1–9. https://doi.org/10.1061/(asce)gt.1943-5606.0002458
Sun, Z., Zhao, Y., Hu, Y., Dias, D., 2023. Probabilistic analysis of width-limited 3D slope in spatially variable soils : UBLA enhanced with efficiency-improved discretization of horn-like failure mechanism. International Journal for Numerical and Analytical Methods in Geomechanics 1–29. https://doi.org/10.1002/nag.3615
Szymkiewicz, F., Guimon-Barrett, A., Marino, J.P., Le Kouby, A., Reiffsteck, P., 2015. Assessment of Strength and Other Mechanical Properties of the Deep Mixing Material, in: Conference Deep Mixing 2015. pp. 651–660.
Tracz, T., Brasse, K., Zdeb, T., Bielecka, J., 2019. Influence of soil-cement composition on its deformability, in: IOP Conference Series: Materials Science and Engineering. p. 538(1): 012010.
Voottipruex, P., Jamsawang, P., Sukontasukkul, P., Jongpradist, P., Horpibulsuk, S., Chindaprasirt, P., 2019. Performances of SDCM and DCM walls under deep excavation in soft clay: Field tests and 3D simulations. Soils and Foundations 59, 1728–1739. https://doi.org/10.1016/j.sandf.2019.07.012
Waichita, S., Jongpradist, P., Jamsawang, P., 2019. Characterization of deep cement mixing wall behavior using wall-to- excavation shape factor. Tunnelling and Underground Space Technology 83, 243–253. https://doi.org/10.1016/j.tust.2018.09.033

Waichita, S., Jongpradist, P., Patawanit, P., Jamsawang, P., Arangelovski, G., Likitlersuang, S., 2021. Deformation and failure mechanism of deep cement mixing walls: experimental study using physical model tests. Archives of Civil and Mechanical Engineering 21, 1–17. https://doi.org/10.1007/s43452-021-00287-3

Waichita, S., Jongpradist, P., Schweiger, H.F., 2020. Numerical and experimental investigation of failure of a DCM-wall considering softening behaviour. Computers and Geotechnics 119, 103380. https://doi.org/10.1016/j.compgeo.2019.103380

Wang, D., Gao, Z., Lee, J.L., Gao, W., 2014a. Assessment and optimization of soil mixing and umbrella vault applied to a cross-passage excavation in soft soils. International Journal of Geomechanics 14, 04014027. https://doi.org/https://doi.org/10.1061/(ASCE)GM.1943-5622.0000374

Wang, D., Olowokere, D., Zhang, L., 2014b. Interpretation of Soil–Cement Properties and Application in Numerical Studies of Ground Settlement Due to Tunneling Under Existing Metro Line. Geotechnical and Geological Engineering 32, 1275–1289. https://doi.org/10.1007/s10706-014-9803-2

Wang, J.H., Xu, Z.H., Wang, W.D., 2010. Wall and Ground Movements due to Deep Excavations in Shanghai Soft Soils. Journal of Geotechnical and Geoenvironmental Engineering 136, 985–994.

Wijerathna, M., Liyanapathirana, D.S., 2018. Reliability-Based Performance of Embankments Improved with Deep Mixing Considering Spatial Variability of Material Properties. ASCE-ASME Journal of Risk and Uncertainty in Engineering Systems, Part B: Mechanical Engineering 4, 1–9. https://doi.org/10.1061/AJRUA6.0000987

Yamashita, K., Hamada, J., Yamada, T., 2011. Field measurements on piled rafts with grid-form deep mixing walls on soft ground. Geotechnical Engineering 42, 1–10.

Yapage, N.N.S., Liyanapathirana, D.S., Kelly, R.B., Poulos, H.G., Leo, C.J., 2014. Numerical Modeling of an Embankment over Soft Ground Improved with Deep Cement Mixed Columns: Case History. Journal of Geotechnical and Geoenvironmental Engineering 140, 1–10. https://doi.org/10.1061/(asce)gt.1943-5606.0001165

Zhang, R., Wu, S., Cao, Y., Guo, Z., 2021. Research on prediction of cement-soil cohesion based on strength test, in: In IOP Conference Series: Earth and Environmental Science. p. 022096. https://doi.org/10.1088/1755-1315/781/2/022096

Zhang, R.J., Hasan, M.S.M., Zheng, J.J., Cheng, Y.S., 2018. Effect of spatial variability of engineering properties on stability of a CSMC embankment. Marine Georesources & Geotechnology 36, 91–99.

Zhang, T., 2023. Deterministic and probabilistic analyses of supported excavations. Université Grenoble Alpes.

Zhang, T., Baroth, J., Dias, D., 2022. Deterministic and probabilistic basal heave stability analysis of circular shafts against hydraulic uplift. Computers and Geotechnics 150, 104922. https://doi.org/https://doi.org/10.1016/j.compgeo.2022.104922

Zhang, T., Baroth, J., Dias, D., Nejjar, K., 2024. Deterministic and probabilistic analysis of great-depth braced excavations: A 32 m excavation case study in Paris. Journal of Rock Mechanics and Geotechnical Engineering 16, 1505–1521. https://doi.org/10.1016/j.jrmge.2023.12.006

Zhang, Z., Ji, J., 2022. Coupling the inverse reliability algorithm with multi-objective reliability-based design optimization of geotechnical systems. Computers and Geotechnics 152, 105005.

Zhao, H., 2022. A practical and efficient reliability-based design optimization method for rock tunnel support. Tunnelling and Underground Space Technology 127, 104587. https://doi.org/10.1016/j.tust.2022.104587

Zhou, J., Ban, C., Zhou, H., Ren, J., Liu, Z., 2023. Experimental Study on the Shear Strength and Failure Mechanism of Cemented Soil–Concrete Interface. Materials 16. https://doi.org/10.3390/ma16124222

Zuo, J., Wang, B., Li, W., Han, S., Wang, J., Zhang, F., 2023. Quality assessment and quality control of deep soil mixing columns based on a cement-content controlled method. Scientific Reports 13, 1–12. https://doi.org/10.1038/s41598-023-31931-y